

Redshift Horizon for Detecting the First Galaxies in Far-Infrared Surveys

MARÍA EMILIA DE ROSSI^{1,2} AND VOLKER BROMM³

¹*Universidad de Buenos Aires, Facultad de Ciencias Exactas y Naturales y Ciclo Básico Común, Buenos Aires, Argentina*

²*CONICET-Universidad de Buenos Aires, Instituto de Astronomía y Física del Espacio (IAFE), Buenos Aires, Argentina*

³*Department of Astronomy, University of Texas at Austin, 2511 Speedway, Austin, TX 78712, USA*

(Received M D, 2019; Revised M D, 2019; Accepted M D, 2019)

Submitted to ApJ

ABSTRACT

We explore the possibility of detecting the first galaxies with the next generation of space-based far infrared (FIR) telescopes by applying an analytical model of primordial dust emission. Our results indicate that FIR/sub-mm sources at $z \gtrsim 7$ will experience a strong negative K-correction. Systems of a given virial mass would exhibit larger dust luminosities at higher z , as a consequence of the increase in dust temperature driven by the higher temperature floor set by the cosmic microwave background. In addition, high- z systems are more concentrated, which enhances the heating efficiency associated with stellar radiation. By analysing source densities as a function of z , and considering survey areas of 0.1 deg^2 and 10 deg^2 , we find that the redshift horizon for detecting at least one source would be above $z \sim 7$ for instrument sensitivities $\lesssim 0.1 - 0.5 \mu\text{Jy}$ and $\lesssim 0.5 - 3.0 \mu\text{Jy}$, respectively, with the exact values depending on the nature of primordial dust. However, galaxy populations with higher than typical metallicities, star formation efficiencies and/or dust-to-metal ratios could relax such sensitivity requirements. In addition, the redshift horizon shows a significant dependence on the nature of primordial dust. We conclude that future FIR campaigns could play a crucial role in exploring the nature of dust and star formation in the early universe.

Keywords: cosmology: theory — dust — galaxies: evolution — galaxies: high-redshift

1. INTRODUCTION

Luminous sources at high redshifts ($7 \lesssim z \lesssim 20$), such as the first galaxies and quasars, constitute promising targets for next-generation surveys as they provide unique tools to test models of early structure formation (Dayal & Ferrara 2018). According to the standard Λ -cold dark matter (Λ CDM) cosmology, the first stellar systems, the so-called Population III (Pop III), formed inside dark matter minihalos of mass $\sim 10^6 M_\odot$ at $z \gtrsim 20$ (e.g., Couchman & Rees 1986; Tegmark et al. 1997; Bromm & Larson 2004; Bromm et al. 2009). However, the low dynamical (virial) masses of these early cosmic structures render them highly susceptible to negative feedback mechanisms that heat the gas, expelling it from their shallow potential wells. Subsequent star

formation is thus subject to quenching or delay (e.g., Muratov et al. 2013; Jeon et al. 2014). If we define a bona-fide galaxy as a long-lived stellar system, the first protogalaxies in the pre-reionization universe could have formed inside the deeper potential wells of atomic cooling halos, with virial masses of $\sim 10^7 - 10^8 M_\odot$ at $z \sim 6 - 15$ (Oh & Haiman 2002; Bromm & Yoshida 2011; Bromm 2013; Safranek-Shrader et al. 2014). In this context, the first supernovae (SNe) would also have engendered the formation of the first dust grains. Detection of thermal dust emission from these primeval sources could thus provide further insight into the nature of primordial star formation (e.g., Valiante et al. 2009; Gall et al. 2011; Jaacks et al. 2018).

The study of dusty star-forming galaxies (DSFGs) has been an active field of research during the last decade (see Casey et al. 2014, for a review). The combined population of DSFGs generates an infrared (IR) radiation field equivalent to the energy density associated to direct stellar emission from galaxies at UV and optical wave-

lengths. Among DSFGs are the most intense starbursts in the universe, reaching star formation rates (SFRs) of $\sim 1000 M_{\odot}\text{yr}^{-1}$ and IR luminosities of $\sim 10^{13} L_{\odot}$. The most luminous of these sources are the brightest galaxies in the universe, and are observed already ~ 800 Myr after the Big Bang. However, luminous IR sources constitute a diverse population, ranging from gas-rich disks to galaxy mergers, with a sub-set harboring heavily dust-enshrouded supermassive black holes (SMBHs). In particular, the discovery of bright sub-millimeter (sub-mm) and IR sources at high- z poses a challenge for models of galaxy formation (e.g., Baugh et al. 2005; Finlator et al. 2006; Fontanot et al. 2007; Davé et al. 2010; Narayanan et al. 2010; Somerville et al. 2012), and it is debated whether they are scaled-up versions of locally observed systems, such as the ultra-luminous infrared galaxies (ULIRGs), or whether they have a different nature (e.g., De Rossi et al. 2018).

At very high redshifts ($z \gtrsim 7$), reprocessed emission from dust heated by stellar UV radiation would be mostly observed at far-IR (FIR) and sub-mm wavelengths. Only sparse and uncertain observations were reported at these extreme distances, with few galaxies and active galactic nuclei (AGN) observed at $z \sim 7 - 8$ (e.g., Mortlock et al. 2011; Venemans et al. 2013), and even fewer at $z \sim 8 - 11$. One of the highest redshift sources was detected by Oesch et al. (2016) at $z \sim 11$, which seems to exhibit a stellar mass of $M_{\star} \sim 2 \times 10^9 M_{\odot}$ and an SFR of $\sim 20 M_{\odot}\text{yr}^{-1}$. In addition, dust continuum has also been reported for a few sources at $z > 6$. Watson et al. (2015) detected a significant amount of dust in a $z \approx 7.5$ galaxy, whose rest-frame UV colors suggested negligible reddening. More recently, Laporte et al. (2017) detected strong mm-continuum flux from a star forming galaxy during the reionization epoch. This source is located at $z \approx 8.4$, hosting a stellar mass of $M_{\star} \sim 2 \times 10^9 M_{\odot}$, an SFR of $\sim 20 M_{\odot}\text{yr}^{-1}$, and a dust mass of $M_{\text{d}} \sim 6 \times 10^6 M_{\odot}$. In addition, Venemans et al. (2017) analysed the [CII] emission and FIR dust continuum in one of the most distant quasars known ($z = 7.1$), using data from the Atacama Large Millimeter/sub-millimeter Array (ALMA). These authors inferred a dynamical mass of $\sim 4 \times 10^{10} M_{\odot}$, and an SFR of $\sim 100 - 350 M_{\odot} \text{yr}^{-1}$ for the host galaxy.

With the advent of new observational facilities to explore the high redshift universe, it is important to provide theoretical models to make predictions about plausible targets, and to guide the development of next-generation instruments. In this regard, Carilli et al. (2017) assessed the prospects for detecting the [CII] $158 \mu\text{m}$ line from distant galaxies, reaching into the ‘dark ages’. At mm wavelengths, and at 6σ significance,

ALMA should be able to detect the [CII] line emission, integrated over 40 h, from an actively star-forming galaxy with moderate metallicity out to $z \sim 10$. The next-generation Very Large Array (ngVLA), planned for 2030 and beyond, will have the sensitivity to detect this emission line from a Milky-Way sized galaxy at $z \simeq 15$. However, the main challenge is the low surface density of high-redshift sources in blind surveys. Employing results from the BLUETIDES simulation, Wilkins et al. (2018) analysed the capabilities of different instruments to study sub-mm sources at $z \gtrsim 8$. They predict that the surface density of $z \gtrsim 8$ sub-mm sources is too low to be detected with *Herschel*, SCUBA-2, or ALMA surveys. Nonetheless, improvements in the area coverage of ALMA could achieve the requirements for detection. The possibility of exploring primeval sub-mm/FIR sources at $z \gtrsim 7$ could be significantly enhanced with the advent of the next generation of space-based FIR telescopes, such as the Origins Space Telescope (OST) or the Space Telescope for Cosmology and Astrophysics (SPICA), planned for launch in the 2030s. Among the key science goals for these facilities will be the cosmic origin of dust, elucidating the first sources of dust emission, which are beyond the current horizon of observability (e.g., Grupponi et al. 2017).

Indeed, the future space-borne FIR telescopes will be ideally complementary to current (e.g., ALMA) and next-generation facilities, such as the *James Webb Space Telescope (JWST)*, which will probe $z \gtrsim 10$ sources in the rest-frame UV. The space-borne missions will be operating in tandem with the suite of extremely large, 30m-class, telescopes on the ground, the Giant Magellan Telescope (GMT), the Thirty-Meter Telescope (TMT), and the European Extremely-Large Telescope (E-ELT). The cold gas at high redshifts will be studied by meter-wavelength radio facilities, focused on the detection of the redshifted 21 cm radiation from neutral hydrogen (Furlanetto et al. 2006; Barkana & Loeb 2007). Among them are the Low Frequency Array (LOFAR), the Murchison Wide-Field Array (MWA), the Precision Array to Probe the Epoch of Reionization (PAPER), the Hydrogen Epoch of Reionization Array (HERA), and ultimately the Square Kilometre Array (SKA).

The main aim of this work is to explore the redshift horizon for dust-emitting galaxies, to be reached with a generic next-generation FIR telescope, considering different instrument sensitivities and survey areas. We apply an analytical model of primordial dust emission in order to evaluate the possibility of detecting primeval FIR/sub-mm sources at $z \gtrsim 7$, given our current understanding of star and galaxy formation at early cosmic

times. Our study is specifically aimed at dust emission from the first galaxies, which formed after Pop III stars enriched the ISM with primordial dust grains. Typical galaxies at these early epochs ($z \approx 7 - 20$) require special modelling as they are not directly related to typical dusty galaxies at lower redshifts, which correspond to a later stage of evolution. These systems typically exhibit very low dust densities, with FIR/sub-mm fluxes below the capabilities of current and near-future instruments (De Rossi & Bromm 2017), rendering their detection very challenging. Future FIR facilities will significantly increase the prospects of achieving the required sensitivity limits. As the nature of the first galaxies is a matter of debate, we explore different dust models and consider systems spanning a wide range of metallicities and dust fractions. The details of such predictions are bound to change, in response to the evolving FIR mission concepts, but it will be useful to establish a baseline exploration.

The plan for the paper is as follows. We discuss our basic theoretical ingredients in Section 2. In Section 3, we analyse the strong negative K-correction affecting high- z sources, followed by a discussion of the minimum halo mass required for detection in Section 4. Our key results for the redshift horizon for different survey parameters are explored in Section 5. In Section 6, we assess the parameter sensitivity of our results. We conclude by comparing our predictions for future FIR facilities with those for the NOEMA, ALMA (Section 7) and the *JWST* (Section 8). A brief summary is presented in Section 9. The following cosmological parameters are assumed in this work: $h = 0.67$, $\Omega_b = 0.049$, $\Omega_M = 0.32$, $\Omega_\Lambda = 0.68$ (Planck Collaboration et al. 2014).

2. METHODOLOGY

To explore the detectability of FIR/sub-mm sources at $z \gtrsim 7$, we apply the model for dust emission from primeval galaxies developed in De Rossi & Bromm (2017). For the convenience of the reader, the model is briefly described in Sections 2.1 and 2.2 (for more details, see De Rossi & Bromm 2017). In Section 2.3, we introduce the methods used to calculate source densities at different redshifts, allowing us to derive the redshift horizon as a function of instrument sensitivity, given our dust model.

2.1. Modelling first galaxies

For modelling a first galaxy, we consider a virialized dark matter halo hosting a central metal-poor Population II (Pop II) stellar cluster, surrounded by a mixed phase of gas and dust. We make the idealized

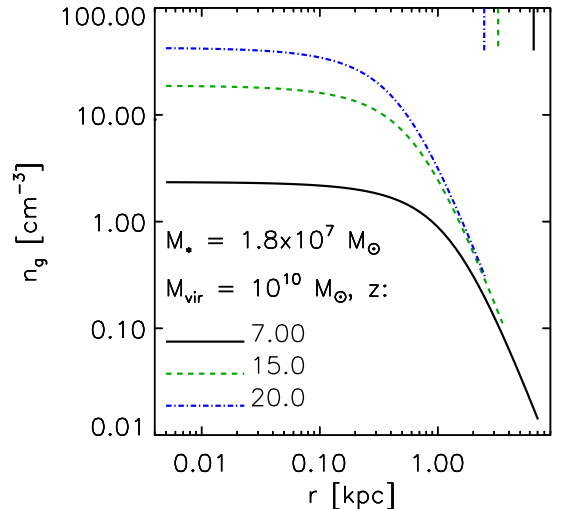


Figure 1. Density structure within the first galaxies. Shown is gas number density as a function of radius, for systems of $M_{\text{vir}} = 10^{10} M_\odot$ and stellar mass $M_* \approx 1.8 \times 10^7 M_\odot$ at different z , as indicated. The vertical lines on the top depict the corresponding virial radii. Evidently, galaxies are more compact at higher z , with important consequences for their intrinsic emissivities.

assumption of spherical symmetry and adopt a gas-density profile of the Burkert (1995) form¹. Following De Rossi & Bromm (2017), the gas profile is defined in such a way that the baryon-to-total mass ratio of a given galaxy is of the order of the cosmic mean (Ω_b/Ω_M). For simplicity, our model does not consider stellar feedback effects, which could expel part of the interstellar medium (ISM) out of the systems; hence, the derived dust luminosities constitute upper limits. In Fig. 1, we show gas density profiles for model galaxies with a virial mass of $M_{\text{vir}} \sim 10^{10} M_\odot$ at select redshifts. The vertical lines on the top indicate the corresponding virial radius, R_{vir} , for each system. It is evident that systems at higher z are more concentrated. In particular, central gas densities are higher by more than one order of magnitude at $z \sim 20$, compared to $z \sim 7$.

To assign the mass of the stellar component, we assume a star formation efficiency of $\eta = M_*/(M_g + M_*) = 0.01$, where M_* and M_g represent the stellar and gas mass, respectively (e.g., Greif & Bromm 2006; Mitchell-Wynne et al. 2015). Considering that the baryon-to-total mass ratio of our primeval sources is of the order Ω_b/Ω_M , the stellar-to-total mass ratio (M_*/M_{vir}) for these systems is about $\approx 2 \times 10^{-3}$. Such

¹ Other density profiles, such as isothermal or Navarro-Frenk-White (NFW), lead to similar results (see De Rossi & Bromm 2017).

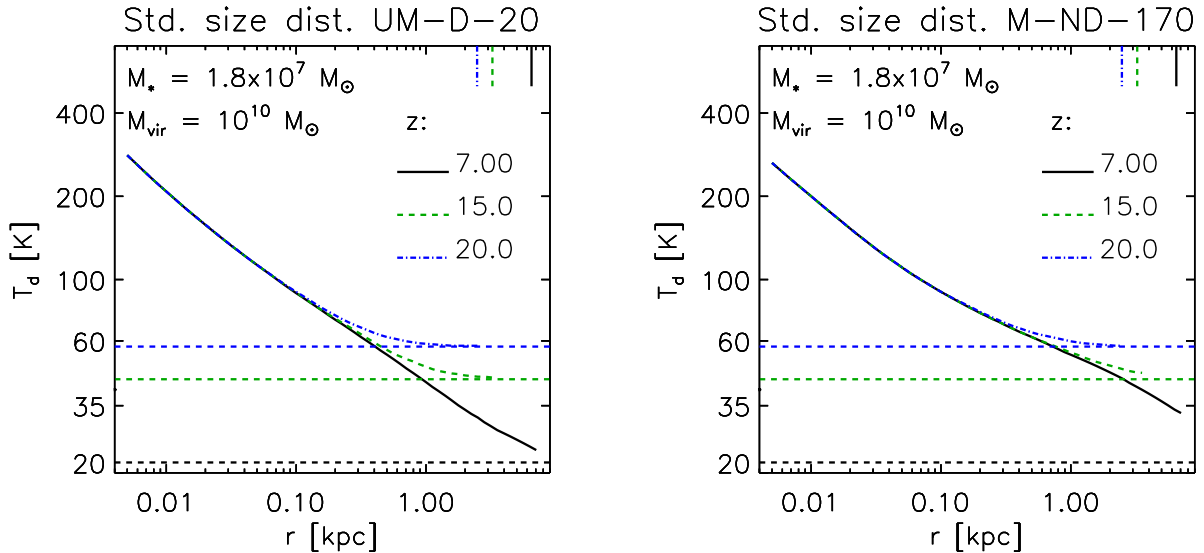


Figure 2. Dust temperature profiles for systems similar to those shown in Fig. 1. The standard size distribution for dust grains is implemented using two different dust chemical compositions: UM-D-20 (left-hand panel) and M-ND-170 (right-hand panel). The horizontal dashed lines denote the CMB temperature at the different redshifts considered. The vertical lines on the top depict the virial radii of these systems.

M_*/M_{vir} corresponds to the minimum value usually derived from models that parametrize the relation between galaxy and halo assembly (e.g., Behroozi et al. 2019). Based on the behavior observed at lower redshifts, extrapolating these models to $z > 7$ and $M_{\text{vir}} \lesssim 10^{13} M_{\odot}$, give M_*/M_{vir} ranging between $\sim 0.001 - 0.1$, with the exact value depending on model details, mass and z . However, given that the estimates of M_* , SFR, and dust content at $z > 4$ remain quite uncertain, the behavior of such quantities at extremely high- z is still vigorously debated. Here, as we are modelling the very *first* galaxies (formed after Pop III stars enriched the ISM with the first metals and dust), we adopt a conservative $\eta = 0.01$ (see Section 6 for results with a higher η).

The spectral energy distribution associated with stars is derived by using Yggdrasil model grids (Zackrisson et al. 2011), corresponding to the lowest available stellar metallicity, $Z_* \approx 3 \times 10^{-2} Z_{\odot}$, and a stellar age $\tau = 0.01$ Myr. To derive dust densities, we adopt a dust-to-metal mass ratio of $D/M = M_{\text{d}}/M_{\text{Z}} = 5 \times 10^{-3}$, and a gas metallicity of $Z_{\text{g}} = 5 \times 10^{-3} Z_{\odot}$. Note that the dust-to-metal ratio here is a global ratio of masses in the system, different from the local ISM density-ratio often considered, with the local ratio being much larger. Our choice of parameters results in a total dust mass that follows the scaling observed in I Zw 18, which is a local analogue of extremely metal-poor galaxies at high redshifts (e.g., Schneider et al. 2016).

2.2. High-redshift dust emission

Following Ji et al. (2014), we consider a suite of different silicon-based dust models, which were calculated by Cherchneff & Dwek (2010) analysing the ejecta of Pop III supernovae: UM-ND-20, UM-ND-170, UM-D-20, UM-D-170, M-ND-20, M-ND-170, M-D-20 and M-D-170.² We acknowledge that there is an ongoing debate to what extent dust at early cosmic times contains a carbon-based component in addition to the silicon-based one. Cherchneff & Dwek (2010) implemented non-equilibrium chemical kinetics for modelling dust formation. In these models, the suppression of carbon dust relies on the hypothesis that carbon-rich regions in the supernova ejecta are microscopically mixed with helium ions. On the other hand, most steady-state models would predict a dominant carbon dust component. It is worth emphasizing that we here focus on the primeval galaxy stage (< 400 Myr since the beginning of star formation), during which stars less massive than $3.5 M_{\odot}$ should not have ejected significant amounts of carbon-enriched material into the ISM.³ As discussed in De Rossi & Bromm (2017), if a moderate contribution of carbon were considered in our model, we would expect

² Model names follow the same notation used in Cherchneff & Dwek (2010): UM = unmixed, M = mixed; ND = non depleted, D = depleted; 170: 170 M_{\odot} progenitor, 20: 20 M_{\odot} progenitor.

³ A similar approach is adopted in De Rossi & Bromm (2017) and De Rossi et al. (2018).

slight variations in the dust temperature and enhanced dust emissivities by a factor of a few.

Cherchneff & Dwek (2010) do not provide grain size distributions for their models. Thus, for modelling the grain size distribution, we consider the so-called “standard” and “shock” prescriptions adopted by Ji et al. (2014). The standard distribution (Pollack et al. 1994) is similar to the Milky Way grain size distribution, while the shock distribution is based on the work of Bianchi & Schneider (2007), approximating the effect of running a post-explosion reverse shock through newly created dust, which leads to smaller grains. Different types of dust would follow likely different size distributions as different chemical species condense to different initial sizes and are subject to different amounts of destruction in a supernova reverse shock (e.g., Todini & Ferrara 2001; Bianchi & Schneider 2007; Nozawa et al. 2007; Silvia et al. 2010). However, as the nature of primordial dust is quite uncertain, for the sake of simplicity, we follow Ji et al. (2014) and assume a similar size distribution for all our dust species. Our aim is not to determine which dust model is more realistic, but to explore the sensitivity of our results on different dust chemistries and grain size distributions. Finally, we note that our model does not consider dust formation in the ISM, as this process is likely to be delayed past the timescale that we consider here, before a significant contribution of carbon dust is injected into the ISM by low mass stars (Asano et al. 2011).

In order to estimate the dust temperature (T_d), we assume thermal equilibrium between the dust cooling and heating rates, the latter given by gas-dust collisions and stellar radiation. As shown by De Rossi & Bromm (2017), photo-heating is the dominant heating mechanism, because of the low ISM densities encountered in the primeval galaxies. The cosmic microwave background (CMB) determines the temperature floor (T_{CMB}), as it is thermodynamically not possible to radiatively cool below it. In Fig. 2, we show T_d profiles for systems similar to those in Fig. 1, but assuming different dust chemical compositions (UM-D-20 and M-ND-170). We adopt a standard size distribution for dust grains; had we used the shock size distribution instead, similar trends would have been obtained, but with slightly higher T_d values (De Rossi & Bromm 2017). In Fig. 2, we see that, for a given M_{vir} and dust model, systems reach higher dust temperatures (T_d) at higher z due to the higher values of T_{CMB} . Also, at higher z , R_{vir} decreases and the density increases towards the center (Fig. 1). Thus, the fraction of dust near the central stellar cluster increases and the heating is more efficient at higher z . Therefore, for systems of similar masses, we

expect larger dust luminosities at higher z , as we will confirm in Section 3.

In order to estimate dust emissivities (j_ν) from the T_d profiles, Kirchhoff’s law was applied:

$$j_\nu(T_d) = 4\pi\kappa_\nu B_\nu(T_d), \quad (1)$$

where κ_ν is the frequency-dependent dust opacity per unit mass, and B_ν is the Planck function.

We estimate the total specific *dust* luminosity, $L_{\nu,\text{em}}$, emitted by a given model galaxy, by integrating j_ν out to R_{vir} . Thus, for a galaxy of a given M_{vir} at redshift z , the observed *dust* specific flux $f_{\nu,\text{obs}}$ originating from the model source is given by:

$$f_{\nu,\text{obs}} = (1+z) \frac{L_{\nu,\text{em}}}{4\pi d_L^2}, \quad (2)$$

where d_L is the luminosity distance to a source at redshift z . As explained below, in order to analyse the possibility of detecting a system of a given M_{vir} at redshift z , we calculate the average $f_{\nu,\text{obs}}$ over the broad FIR band $\Delta\lambda = 250 - 750 \mu\text{m}$ and compare it with a potential range of detector sensitivities at similar wavelengths.

It is worth mentioning that our dust model has been successfully applied to predict the FIR spectral energy distribution (SED) of first massive galaxies at $z \gtrsim 5$ (De Rossi et al. 2018). In particular, adapting the model to conditions in FIR galaxies at $z \sim 6$ and adding a low percentage of carbon dust, De Rossi et al. (2018) were able to reproduce the SED of Haro 11, which is a local galaxy with a moderately-low metallicity, an exceptionally high star formation rate and a very young stellar population, which likely approximates the relevant conditions in young massive Pop II galaxies at high z . These authors conclude that there seems to be a progression with redshift in observed galaxy SEDs, from those resembling local ones at $1 < z < 4$ to a closer resemblance to Haro 11 at $5 \lesssim z < 7$.

Typical rest-frame and observed spectra of model galaxies at $z \gtrsim 7$ in the context of potential detections with next-generation FIR facilities are presented and discussed in Section 3.

2.3. Source densities

Our goal is to estimate the redshift horizon for a generic FIR telescope, considering the sensitivity limits required to detect the weak continuum radiation from primordial dust, in the context of our current understanding of first galaxy formation. The redshift horizon (z_{lim}) is defined as the highest z above which the projected number of sources per given solid angle ($\Delta\Omega$) is $N \leq N_{\text{crit}}$, where we here consider $N_{\text{crit}} = 1$.

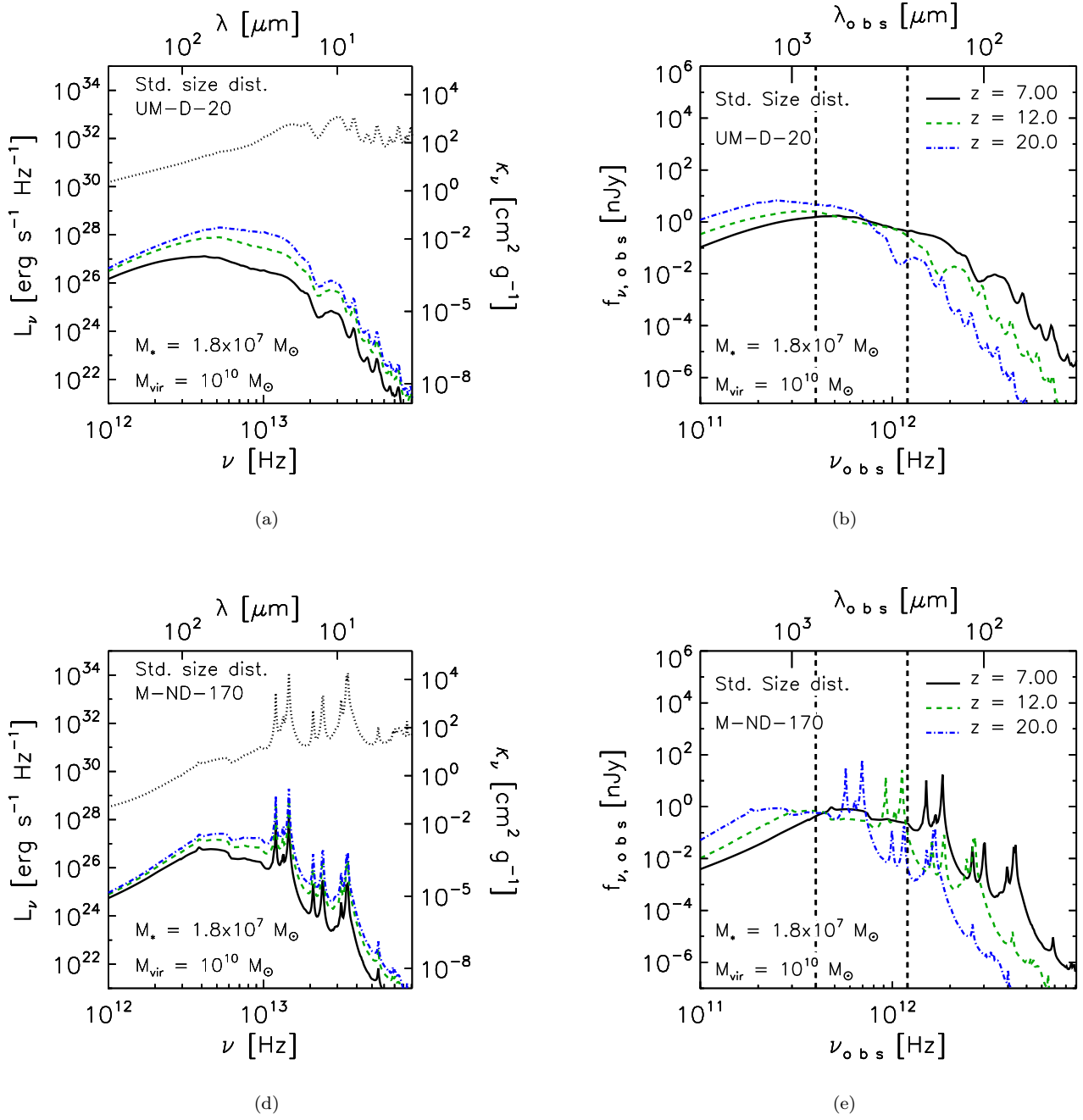


Figure 3. Dust re-emission spectra for the same systems shown in Fig. 2, all having $M_{\text{vir}} = 10^{10} M_\odot$ and $M_* \approx 1.8 \times 10^7 M_\odot$, at different z . Left-hand panels: rest-frame spectra for individual sources. The dotted black curves depict the frequency-dependent dust opacities, κ_ν , corresponding to the different dust models. Right-hand panels: observed specific fluxes. Vertical dashed lines indicate the FIR frequency range which was adopted in this work.

For simplicity, we assume that the observed number of sources per unit redshift per unit solid angle is given by

$$\frac{dN}{dzd\Omega} = \int_{M_{\min}}^{\infty} \frac{dN}{dM dV} \frac{dV}{dz d\Omega} dM = \int_{M_{\min}}^{\infty} n_{\text{ST}} r^2 \frac{dr}{dz} dM, \quad (3)$$

where dV is the comoving volume element, and n_{ST} the Sheth-Tormen mass function⁴ (Sheth et al. 2001). The comoving distance to redshift z is given by

$$r(z) = \frac{c}{H_0} \int_0^z \frac{dz'}{\sqrt{\Omega_m(1+z')^3 + \Omega_\Lambda}}, \quad (4)$$

where c/H_0 is the present-day Hubble distance.

For a given instrument sensitivity (S), M_{\min} is defined as the virial mass corresponding to the least massive systems which could be detected at FIR/sub-mm wavelengths at redshift z . To estimate M_{\min} , we calculate the FIR/sub-mm observed fluxes for our model galaxies as a function of mass and z (see Section 2.2, Equ. 2), and compare them with the detector sensitivity at similar wavelengths. To obtain an estimate of the potential observed FIR/sub-mm fluxes (F_{FIR}), we average the model spectra over the broad FIR band $\Delta\lambda = 250 - 750 \mu\text{m}$, where we approximate $\Delta\lambda \sim \lambda$:

$$F_{\text{FIR}} = \frac{\int_{\nu_i}^{\nu_f} f_{\nu, \text{obs}} d\nu_{\text{obs}}}{\nu_f - \nu_i}. \quad (5)$$

ν_i and ν_f correspond to the frequency range associated to our adopted FIR filter. To render our results applicable for different sets of instrument parameters, we analyse results for a wide range of sensitivities ($S = 10^{-3} - 10^3 \mu\text{Jy}$), but we note that a sensitivity of $\sim 1 \mu\text{Jy}$ would be a more realistic value for the next decades. Therefore, M_{\min} is estimated as the lowest M_{vir} such that $F_{\text{FIR}} \geq S$, where $S \equiv S(t)$ represents the detector sensitivity for a given exposure time t . As F_{FIR} depends on the adopted dust model, M_{\min} and the source density will also be affected by the adopted dust prescriptions.

The projected number of sources within a solid angle $\Delta\Omega$ at redshift z is defined as

$$N(> z) = \Delta\Omega \int_z^{z_{\max}} \frac{dN}{dz' d\Omega} dz', \quad (6)$$

where $\Delta\Omega$ represents the observed region of the sky, and z_{\max} corresponds to the maximum z where

⁴ The Sheth-Tormen formalism provides a better fit to simulations than the Press-Schechter (PS) approach, which underpredicts the abundance of halos at high redshifts.

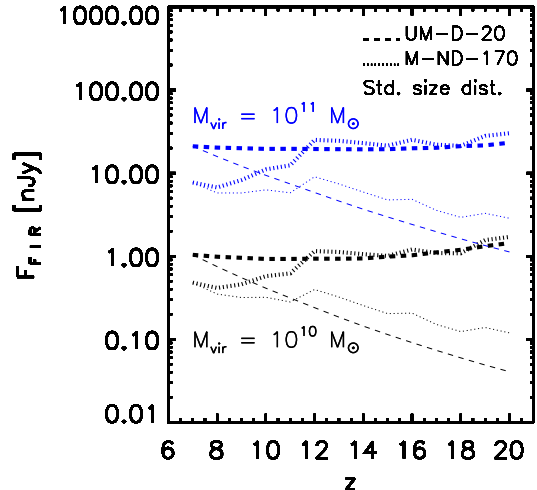


Figure 4. FIR flux for galaxies of different masses ($M_{\text{vir}} = 10^{10}$ and $10^{11} M_{\odot}$, corresponding to $M_* \approx 1.8 \times 10^7$ and $1.8 \times 10^8 M_{\odot}$, respectively) as a function of redshift (thick lines). Results correspond to the same dust models analysed in Fig. 3. In order to show the effects of the strong negative K-correction affecting these galaxies, thin lines depict the FIR flux obtained assuming that galaxies with similar masses exhibit the same ($z = 7$) rest-frame specific luminosity at all redshifts.

the first galaxies could have formed. Following De Rossi & Bromm (2017), we adopt $z_{\max} = 20$. We will, particularly, focus on the cases $\Delta\Omega = 0.1, 1.0$ and 10 deg^2 , which correspond to potential ultra-deep, deep and medium survey areas in the FIR.

We emphasize that our adopted sensitivities and survey areas cover a wide range of plausible values in order to be useful for different potential FIR observational campaigns.

3. FIRST GALAXY K-CORRECTION

In this section, we implement the methodology described in Section 2 to discuss the strong negative K-correction, affecting dust emission at extremely high z . We show that such K-correction effects significantly enhance the capabilities of a generic FIR telescope to detect the dust continuum emission from primeval galaxies at $z = 7 - 20$.

In Fig. 3, we show the dust re-emission spectra for the same systems shown in Fig. 2, all with $M_{\text{vir}} = 10^{10} M_{\odot}$ and $M_* \approx 1.8 \times 10^7$, at different z . The rest-frame spectra for individual sources are plotted in the left-hand panels. The dotted black curves depict the frequency-dependent dust opacities, κ_{ν} , corresponding to the different dust models. The distinct spectral features reflect the properties of the underlying opacity curves. Interestingly, at a fixed $M_{\text{vir}} = 10^{10} M_{\odot}$, the maximum lu-

minosity increases with z , with galaxies being ~ 1 order of magnitude brighter at $z \approx 20$ compared to similar galaxies at $z \approx 7$. This behaviour is consistent with the T_d profiles shown in Fig. 2. As we anticipated, higher dust temperatures are expected at high redshifts due to the higher intensity of the CMB. Also, systems of similar M_{vir} exhibit smaller R_{vir} at higher z . Thus, a larger fraction of dust is located in the surroundings of the central stellar cluster at higher z , leading to a more efficient heating of dust grains. All these effects result in an increased dust emissivity with increasing z . Thus, our findings suggest that the first galaxies would experience a strong negative K-correction, thus facilitating their detectability.

In the right-hand panel of Fig. 3, we show observed specific fluxes, predicted for the two dust models described above. The vertical dashed black lines depict the FIR wavelength band adopted in this work to estimate the average FIR/sub-mm radiation (see Section 2). As can be seen, at a given mass, the observed flux reaches higher values at higher z , despite the larger luminosity distance to the observer. As explained before, the higher dust temperature achieved at higher z compensates for the distance effect. We also note that main spectral features enter the FIR band in the $z \sim 12 - 20$ range. Thus, observations in the FIR would be sensitive to such spectral features, as well.

In order to more fully explore the effects of the strong negative K-correction affecting primeval galaxies, Fig. 4 compares the FIR flux predicted by our model (thick lines) with the FIR flux obtained assuming that model galaxies with similar masses exhibit the same ($z = 7$) rest-frame specific luminosity at all redshifts (thin lines). Results for galaxies of different masses (10^{10} and $10^{11} M_{\odot}$, corresponding to $M_* \approx 1.8 \times 10^7$ and $1.8 \times 10^8 M_{\odot}$, respectively) are shown and correspond to the same dust models analysed in Fig. 3. In the case of the UM-D-20 model, which leads to weaker spectral features (Fig. 3), the negative K-correction generates an almost constant FIR flux at $z = 7 - 20$, while, for the M-ND-170 model, associated to stronger spectral features, the flux remains almost constant at $z = 12 - 20$ and decreases by a factor of 2 towards $z = 7$ (thick lines). In the latter case, the higher FIR fluxes at $z = 12 - 20$ is explained by the main spectral features that enter the FIR filter ($\Delta\lambda = 250 - 750 \mu\text{m}$) at $z \gtrsim 12$ (see Fig. 3). If K-correction effects were not present (thin lines), the FIR flux associated to the UM-D-20 (M-ND-170) model would decrease by a factor of ~ 10 (~ 2) between $z = 7$ and 20. At $z = 20$, it is clear that the strong negative K-correction leads to an increase of the observed flux by ~ 1 order of magnitude for both considered mod-

els. Similar trends are obtained for the whole range of masses associated to first galaxies ($M_{\text{vir}} > 10^7 M_{\odot}$).

In Fig. 5, we analyse the FIR flux as a function of M_{vir} and M_* for the same dust chemical models used in Fig. 3. Left- and right- hand panels show results for a standard and shock size distributions of dust grains, respectively. Predictions for $z = 7$ (black lines) and $z = 20$ (blue lines) are compared. Intermediate trends are obtained at intermediate redshifts ($7 < z < 20$). As expected from Fig. 4, the $F_{\text{FIR}} - M_{\text{vir}}$ relation associated to the UM-D-20 dust model seems not to evolve with z ; i.e., systems of a given mass present similar observed fluxes, regardless of their redshift. On the other hand, the $F_{\text{FIR}} - M_{\text{vir}}$ relation corresponding to the M-ND-170 model moves towards lower fluxes at lower z (see also Fig. 4); thus, contrary to expectations, systems with similar masses are brighter if they are located at higher z . Thus, a strong negative K-correction is also evident here. Horizontal dashed lines in Fig. 5 denote select characteristic sensitivity values ($S = 0.1, 1$ and $10 \mu\text{Jy}$), covering the scope of future FIR surveys. We see that masses of $M_{\text{vir}} \gtrsim 10^{11} - 10^{12} M_{\odot}$ and $M_* \gtrsim 1.8 \times 10^8 - 1.8 \times 10^9 M_{\odot}$ ($M_{\text{vir}} \gtrsim 10^{13} - 10^{14} M_{\odot}$ and $M_* \gtrsim 1.8 \times 10^{10} - 1.8 \times 10^{11} M_{\odot}$) are required to reach sensitivity limits of $S \sim 0.1 \mu\text{Jy}$ ($S \sim 10.0 \mu\text{Jy}$), with the exact value depending on dust properties. In the next section, we will discuss the minimum mass required for detecting primeval sources in greater detail.

4. MINIMUM MASS LIMIT

In Section 3, we found that primeval FIR/sub-mm sources experience a significant negative K-correction. In this section, we determine the minimum galaxy mass required for detection with a generic FIR telescope, as a function of z and for different dust models.

In Fig. 6, we predict the virial mass limit, M_{min} , for detections as a function of z (see Sec. 2). As a reference, right vertical axes show the associated stellar mass values adopting our conservative star formation efficiency $\eta = 0.01$. Predictions of different dust models for the standard (left) and shock (right) dust size distributions are shown, as indicated in the figure. An instrument sensitivity of $1 \mu\text{Jy}$ at $\lambda_{\text{obs}} = 250 - 750 \mu\text{m}$ has been assumed, which is a plausible value for a potential ultra-deep blind survey in the next decades. For the sake of comparison, we show curves depicting halo masses for different overdensities ($\nu\text{-}\sigma$ peaks) in the underlying Gaussian field of cosmological density fluctuations.

For clarity, Fig. 6 does not show the $M_{\text{min}} - z$ relations for different sensitivity values, but such scalings can be easily inferred by combining data from Fig. 5 and 6. We note that, according to Fig. 6, dust models UM-D-20 and

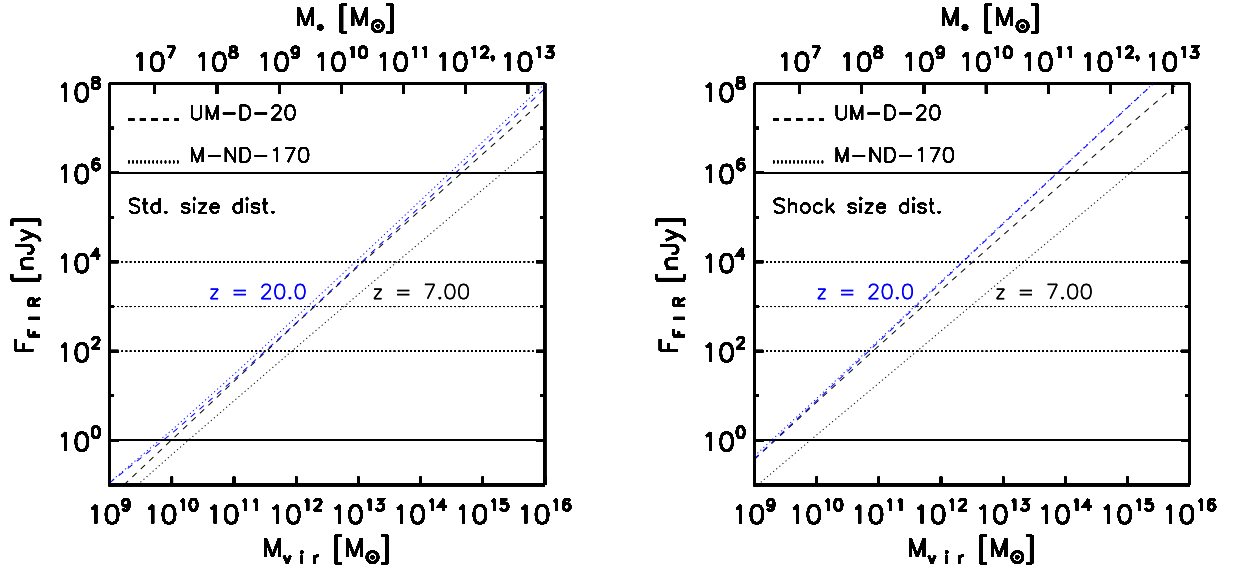


Figure 5. FIR flux as a function of M_{vir} (bottom horizontal axis) and M_* (top horizontal axis) for the same dust models shown in Fig. 3 in the case of a standard (left-hand panel) and shock (right-hand panel) size distributions. Results for $z = 7$ (black lines) and $z = 20$ (blue lines) are compared. Horizontal dashed lines denote select sensitivity values (0.1, 1 and 10 μJy) that will be considered for analysing the potential detection of first galaxies. Horizontal solid lines enclose the whole range of sensitivity values considered in this work.

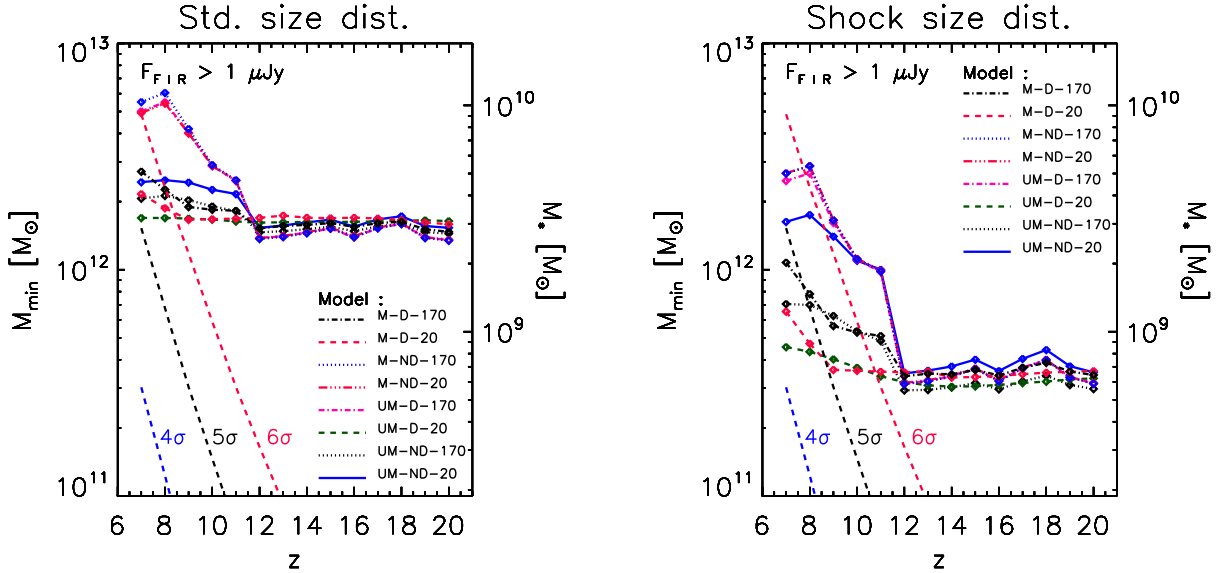


Figure 6. Lowest virial mass (left vertical axis) required for detection as a function of z , assuming a sensitivity of $1\mu\text{Jy}$. Right vertical axes show the associated stellar mass values adopting our conservative star formation efficiency $\eta = 0.01$. Predictions for different dust models are shown: standard (left) and shock (right) dust size distributions, as indicated in the figure. For comparison, different ν - σ peaks corresponding to the adopted cosmological model are plotted.

M-ND-170 lead to the lowest and highest M_{\min} values for a given z and size distribution, with all other models exhibiting an intermediate behaviour. Furthermore, we find that, in general, different models exhibit similar $M_{\min} - z$ curves for different sensitivity values, but with an increase of the M_{\min} normalization for higher sensitivities. Thus, for models UM-D-20 and M-ND-170, the M_{\min} normalization can be derived from Fig. 5 by determining where the corresponding $F_{\text{FIR}} - M_{\text{vir}}$ curves (at $z = 7$ and 20) cross the horizontal line depicting a given sensitivity S . As models UM-D-20 and M-ND-170 represent upper and lower limits for M_{\min} , the M_{\min} normalization (associated to sensitivity S), for the remaining chemical models, would lie approximately between these two extreme cases.

Comparing left- and right-hand panels in Fig. 6, we note that M_{\min} is lower for the shock size distribution of dust grains, which is explained by the higher F_{FIR} fluxes obtained in this case (Fig. 5). As discussed in De Rossi & Bromm (2017), the shock size distribution leads to higher T_{d} and dust emissivities, which is consistent with the aforementioned behaviour. In the case of the standard size distribution, $M_{\min} \approx 1 - 2 \times 10^{12} M_{\odot}$ at $z \gtrsim 12$, while for the shock size distribution, $M_{\min} \approx 3 - 4 \times 10^{11} M_{\odot}$ at similar z . The extreme negative K-correction, as noted previously, leads to a lowest value of M_{\min} at $z \gtrsim 12$. In addition, we find another unexpected behaviour, seen at $z \lesssim 12$: M_{\min} increases towards lower z , depending on the dust model. In the case of the standard size distribution, M_{\min} reaches a maximum of $\approx 6 \times 10^{12} M_{\odot}$ at $z \lesssim 8$, when applying the M-ND-170 dust chemistry. For the same dust chemistry, but implementing the shock size distribution, M_{\min} reaches its maximum of $\approx 3 \times 10^{12} M_{\odot}$ at $z \lesssim 8$. However, other dust chemistries, such as the UM-D-20 model, only show modest variations of M_{\min} at $z \lesssim 12$.

The peculiar trends obtained at $z \approx 7 - 12$ can be explained again (see also Section 3) by analysing the predicted spectra shown in Fig. 3. There, we compare the energy distributions associated with the UM-D-20 and M-ND-170 models. The former exhibit the lowest M_{\min} at $z = 7$, and the latter the highest M_{\min} at the same z (Fig. 6). By comparing the spectra corresponding to these two extreme cases, it is clear that differences between the average fluxes (F_{FIR}) are driven by the different redshifted spectral features that enter the wavelength range corresponding to our fiducial FIR filter ($\Delta\lambda = 250 - 750 \mu\text{m}$, vertical dashed black lines in Fig. 3) at a given z . At $z > 12$, both dust models exhibit similar values of M_{\min} because, at those z , all the main spectral features have entered the adopted FIR band. At $z < 12$, the average flux evolves, as different spectral fea-

tures enter the FIR band. The model UM-D-20, which exhibits weaker features, does not evolve significantly over the whole z range. On the other hand, the model M-ND-170, which exhibits stronger features, shows more significant evolution at $7 < z < 12$. The dust spectral features are associated with the underlying dust opacities, and therefore depend on dust chemical composition. According to these findings, the chemical composition of dust in primordial galaxies at $z = 7 - 12$ might affect their detection at FIR/sub-mm wavelengths. Future telescopes operating in this wavelength range and with low enough sensitivities could, thus, constrain the nature of dust in the early universe.

Although the strong negative K-correction, found for FIR/sub-mm sources at early times, enhances their chances of being detected, halos with $M_{\text{vir}} > M_{\min} > 10^{11} M_{\odot}$ are extremely rare at high z . To illustrate this fact, the $M_{\text{vir}} - z$ curves for different $\nu - \sigma$ overdensities are overplotted in Fig. 6. We see that systems with $M_{\text{vir}} > M_{\min}$ are far from typical at those redshifts, representing highly biased overdensities. Fig. 6 shows results for a sensitivity of $1 \mu\text{Jy}$. Even if we consider extreme sensitivities of 1 nJy , a minimum mass of $\gtrsim 10^9 M_{\odot}$ (see Fig. 5) would be required for detection, above a $2 - \sigma$ peak at these high redshifts. As our model sources represent the first galaxies hosting primordial dust grains, their dust masses are very low and high masses are required to achieve detectable fluxes at FIR/sub-mm wavelengths (e.g., Jaacks et al. 2018). Thus, although possible, detecting these systems in the dust continuum would be difficult with blind surveys. However, we acknowledge significant uncertainties regarding the nature of primeval galaxies and their dust content. In Section 6, we show that an increase of our adopted values of D/M , Z_{g} or η would lead to lower values of M_{\min} , enhancing the chances of detecting the dust emission from first galaxies. As discussed below, gravitational lensing could also be a crucial tool for detecting the most elusive faint sources, and such analysis will be the subject of a forthcoming study.

Next, we analyse the probability of individual detections during potential blind surveys considering different instrument sensitivities and survey areas.

5. THE REDSHIFT HORIZON

Following the procedures described in Section 2.3, in this section, we derive the projected number of sources (Equ. 6) as a function of z during potential blind surveys, assuming observations with different instrument sensitivities and considering different survey areas. Note that we only consider redshifts ranging from 7 to 20,

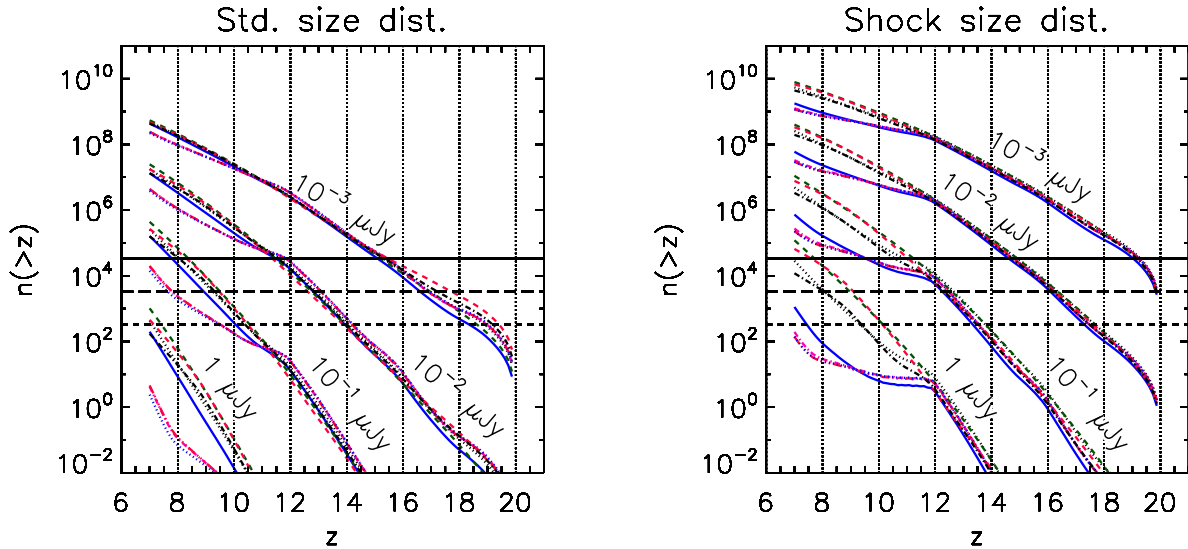


Figure 7. Number of sources per steradian above redshift z detected during potential surveys. Results for different sensitivity values are explored, as indicated in the figure. Results for the standard (left-hand panel) and shock (right-hand panel) grain size distributions are shown. Different dust models (see Fig. 6 for line style convention) are considered. The horizontal lines depict the regions corresponding to the redshift horizon ($n(> z_{\text{lim}}) = 1/\Delta\Omega$) considering survey areas of $\Delta\Omega = 0.1$ (solid line), 1.0 (long-dashed line) and 10 deg^2 (dashed line), respectively.

as these are the plausible times when the first galaxies could have formed.

Fig. 7 shows the number of sources per steradian above redshift z ($n(> z)$) which could be detected during potential surveys. Results for the standard (left-hand panel) and shock (right-hand panel) grain size distributions are shown and different dust chemical models (see Fig. 6 for line style convention) are considered. The horizontal lines depict the regions corresponding to the redshift horizon ($n(> z_{\text{lim}}) = 1/\Delta\Omega$) considering survey areas of $\Delta\Omega = 0.1$ (solid line) and 10 deg^2 (dashed line), respectively. Results for different sensitivity values are explored: $S = 1, 10^{-1}, 10^{-2}$ and $10^{-3} \mu\text{Jy}$. Curves associated with sensitivities greater than $\sim 1 \mu\text{Jy}$ do not reach the horizon for the adopted survey areas; hence, for the sake of clarity, these curves were not plotted.

As expected from Fig. 6, Fig. 7 shows that higher source densities are obtained for the shock size distribution, reaching differences of more than one order of magnitude. Regarding the dust chemical composition, it also affects source densities, with a larger impact when the shock size distribution is adopted. In particular, we see that, for a given size distribution and sensitivity S , different dust chemistries lead to similar $n(> z) - z$ curves at $z > 12$. On the other hand, at $z < 12$, $n(> z)$ exhibits a more significant dependence on the dust chemical composition. The latter behavior is a consequence of the dependence of M_{min} on the dust chemistry at $z < 12$ (see

Sec. 4), which is caused by the different spectral features that enter the adopted FIR filter at $z < 12$ for different models. Thus, our findings suggest that the number of detected sources depends on the properties of primordial dust and, hence, measurements of source densities might provide important constraints on the nature of dust chemical composition and grain size distributions at very early cosmic times.

According to Fig. 7, the probability of detecting one individual source exhibiting *typical* properties expected for first galaxies depends mainly on the instrument sensitivity and, secondly, on the survey area. In the case of the shock size distribution, the redshift horizon for $S \sim 1 \mu\text{Jy}$ is reached at $z \sim 7 - 10$, with the exact value depending on $\Delta\Omega$ and dust chemical composition. In the case of the standard size distribution, the redshift horizon for $S \sim 1 \mu\text{Jy}$ only reaches $z \sim 7$ for $\Delta\Omega = 10 \text{ deg}^2$ and for some particular dust chemistries. For instrument sensitivities $S \lesssim 0.1 \mu\text{Jy}$ and $\Delta\Omega \gtrsim 0.1 \text{ deg}^2$, all dust models predict a redshift horizon above $z \approx 7$.

Fig. 8 summarizes our findings regarding the redshift horizon (z_{lim}) as a function of sensitivity (S) for different survey areas and dust models. For the standard size distribution, the $z_{\text{lim}} - \log_{10}(S)$ relation at $z_{\text{lim}} > 12$, approximately follows a relation of the form $z_{\text{lim}} = -4 \log_{10}(S/n\text{Jy}) + z_{\text{lim}}(S = 1 \text{ nJy})$, where $z_{\text{lim}}(S = 1 \text{ nJy}) \approx 15, 17$ and 18 , for $\Delta\Omega = 0.1, 1$ and 10 deg^2 , respectively. A similar relation, with roughly the same slope, is obtained for the shock size distribu-

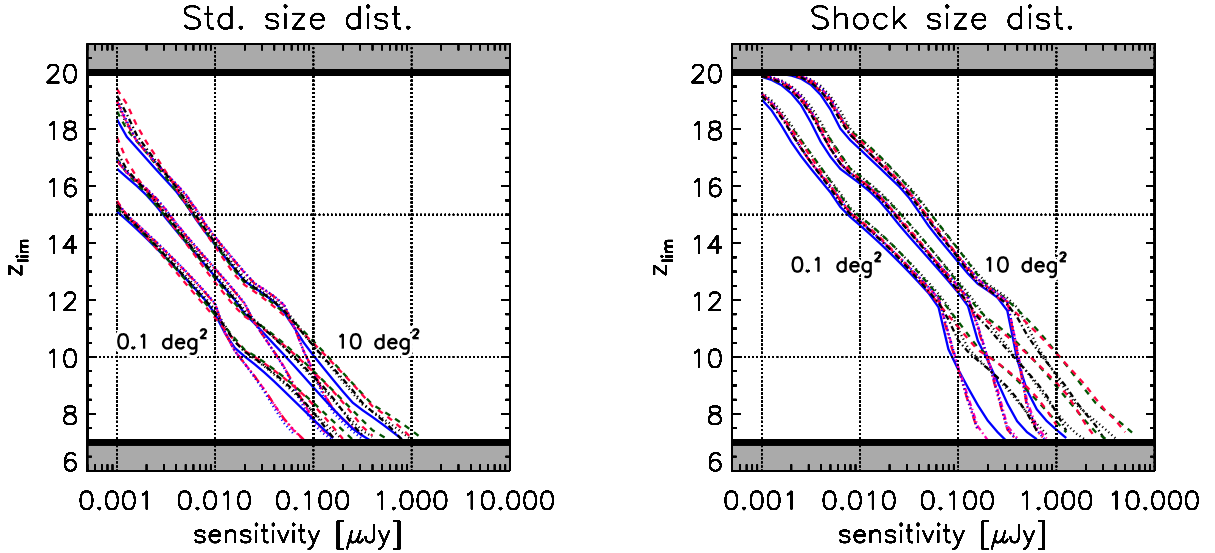


Figure 8. Redshift horizon as a function of instrument sensitivity for three different survey areas: 0.1, 1.0 and 10.0 deg^2 , as indicated in the figure. Results for the standard (left-hand panel) and shock (right-hand panel) grain size distributions are shown. Different dust models (see Fig. 6 for line style convention) are considered. Our analysis is restricted to $z = 7 - 20$, where first galaxies are expected to form.

tion at $z_{\text{lim}} > 12$, but with $z_{\text{lim}}(S = 1 \text{ nJy}) \approx 19, 20$ and 21.5, for $\Delta\Omega = 0.1, 1$ and 10 deg^2 , respectively. At $z < 12$, the $z_{\text{lim}} - \log_{10}(S)$ curves depart from linearity for some dust models as their associated spectral features enter our adopted FIR filter (see Sec. 4). Only models with weak spectral features (e.g. UM-D-20) predict a linear behavior along the whole redshift range associated with first galaxy formation.

Considering our whole set of plausible dust models, a sensitivity $S \lesssim 0.1 \mu\text{Jy}$ and a survey area $\Delta\Omega \gtrsim 0.1 \text{ deg}^2$ are required in order to assure the detection of the dust continuum emission of at least one individual first galaxy during a FIR survey at $z > 7$. However, depending on the exact properties of primordial dust, a redshift horizon $z_{\text{lim}} \gtrsim 7$ could be also achieved for sensitivities $S \lesssim 10 \mu\text{Jy}$ ($S \lesssim 1 \mu\text{Jy}$) and $\Delta\Omega \gtrsim 10 \text{ deg}^2$ ($\Delta\Omega \gtrsim 0.1 \text{ deg}^2$). Finally, only in the case of a shock size distribution of dust grains, the maximum redshift horizon $z_{\text{lim}} \approx 20$ could be reached for an extreme sensitivity $S \sim 1 \text{ nJy}$ and $\Delta\Omega = 0.1 - 10 \text{ deg}^2$.

Although our findings suggest that the probability of detecting *typical* first galaxies in blind surveys will be very challenging, given the extreme sensitivities required, the nature of primordial galaxies is still uncertain and we will show that observational prospects increase significantly with the metallicity and dust-to-metal ratio of the considered model sources (Section 6).

6. PARAMETER SENSITIVITY

The nature of primordial dust and its host galaxies is still a matter of debate. In order to estimate the uncertainties of our model predictions, we evaluate the effects of varying the more critical parameters. In the following, for the sake of clarity, only results for the UM-ND-20 model are shown as this model exhibits an intermediate behavior (see Fig. 6 and 7). All other models predict similar trends but with slight variations in the normalization of M_{min} and $n(> z)$ at $z < 12$. In Fig. 9, we show the impact of variations of different model parameters on the $M_{\text{min}} - z$ (left-hand panel) and $n - z$ (right-hand panel) relations. For the sake of comparison with Fig. 6 and 7, we adopted an instrument sensitivity $S = 1 \mu\text{Jy}$. As discussed before, if varying the sensitivity, similar curves are obtained but with a change in the absolute normalization of the relations (Figs. 5, 6 and 7).

For evaluating the effects of the dust-to-metal ratio, we consider the cases: $D/M = 0.005$ (reference), 0.06 and 0.4 (Cen & Kimm 2014). We can see that M_{min} decreases almost proportionally to the increase of D/M . This is consistent with the results in De Rossi & Bromm (2017), who reported that the dust radiation intensity increases nearly linearly with the dust fraction. In particular, for the extreme value of $D/M = 0.4$ and a shock size distribution, $M_{\text{min}} = 1 - 10 \times 10^{10} M_{\odot}$. We also tested the effects of changing the gas metallicity to $Z_{\text{g}} = 5 \times 10^{-4}$, 5×10^{-3} (reference) and $5 \times 10^{-2} Z_{\odot}$. As noted by De Rossi & Bromm (2017), D/M and Z_{g} are degenerate parameters, with M_{min} increasing almost

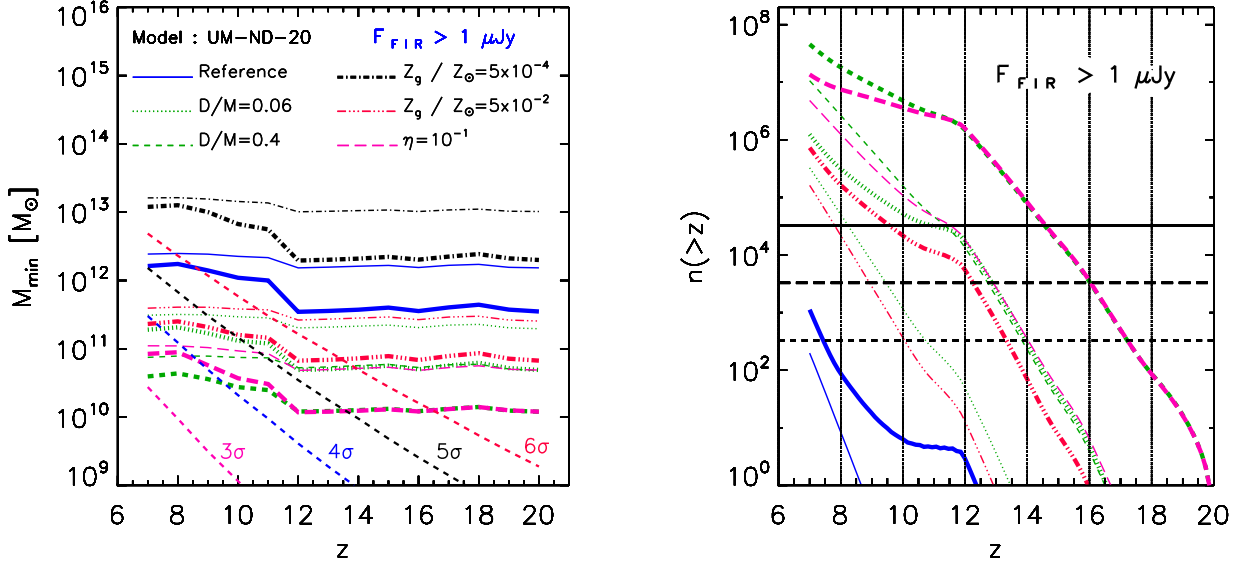


Figure 9. Impact of varying model parameters on the $M_{\min} - z$ (left-hand panel) and $n - z$ (right-hand panel) relations, adopting a sensitivity $S = 1 \mu\text{Jy}$ (compare with Fig. 6 and 7, respectively). We only show results for the UM-ND-20 model, to emphasize the key features. Thin and thick lines are associated with the standard and shock size distributions, respectively. The reference model (solid blue line) corresponds to our standard parameters (De Rossi & Bromm 2017). The effects of variations of model parameters with respect to the standard model are shown with different line styles. Note that, in the right-hand panel, the curves corresponding to the case $Z_g = 5 \times 10^{-4} Z_{\odot}$ (dot-dashed lines) are not shown as they lie below the plotted region. For $\eta = 0.1$, $M_*/M_{\min} \approx 2 \times 10^{-2}$, while, for the rest of the models, $M_*/M_{\min} \approx 2 \times 10^{-3}$.

proportionally to the decrease of Z_g . For the extreme lowest value of $Z_g \approx 5 \times 10^{-4} Z_{\odot}$ and a standard distribution for dust grains, M_{\min} reaches the highest value of $\approx 10^{13} M_{\odot}$. For $Z_g \approx 5 \times 10^{-2} Z_{\odot}$, we obtain similar changes to those derived from using $D/M = 0.06$. To explore the impact of the adopted star formation efficiency, we increased η to the extreme value of 0.1. We note that, for $\eta = 0.1$, the stellar-to-total mass ratio is $M_*/M_{\min} \approx 2 \times 10^{-2}$, while, as previously discussed, for the rest of the models explored in this work, $M_*/M_{\min} \approx 2 \times 10^{-3}$. As a higher η would drive an enhanced ISM metallicity, we also increased Z_g to $0.05 Z_{\odot}$, consistent with the closed-box model approximation: $Z = -y \ln(1 - \eta)$, where y is the stellar yield. Although this approximation might not describe the real behavior of these sources, it provides an upper limit for the predicted dust emission. We see that these changes lead to a lower M_{\min} , obtaining similar results to those derived when increasing D/M to the extreme value of 0.4. In summary, variations of model parameters to extremely low and high values lead to significant changes in M_{\min} , resulting in variations of more than two orders of magnitude.

With respect to the number density of sources, $n(> z)$, a similar sensitivity is seen when varying model parameters to extreme values. For $Z_g = 5 \times 10^{-4} Z_{\odot}$, the probability of detecting one primeval source, assuming

$S \sim 1 \mu\text{Jy}$ and $\Delta\Omega \lesssim 10 \text{ deg}^2$, is below unity ($n(> z) < 1/\Delta\Omega$) at all redshifts $z \geq 7$. In the case of our default metallicity value ($Z_g = 5 \times 10^{-3} Z_{\odot}$) and adopting $\Delta\Omega \lesssim 10 \text{ deg}^2$, this probability increases to 1 at $z \approx 7$. On the other hand, for $D/M \gtrsim 0.06$, $Z_g \gtrsim 5 \times 10^{-2} Z_{\odot}$ or $\eta = 0.1$, and assuming $S \sim 1 \mu\text{Jy}$, the redshift horizon, defined as the redshift where $n(> z) = 1/\Delta\Omega$, extends towards $z \gtrsim 7$ for our whole range of considered survey areas ($\Delta\Omega = 0.1 - 10 \text{ deg}^2$). In the case of a standard size distribution and for $D/M \sim 0.06$ or $Z_g \sim 5 \times 10^{-2} Z_{\odot}$, the redshift horizon is reached at $z \approx 8, 9$ and 10 for $\Delta\Omega \approx 0.1, 1$ and 10 deg^2 , respectively. In the case of a shock (standard) size distribution and an extreme value of $D/M \sim 0.4$ or $\eta = 0.1$, the redshift horizon extends towards $z \sim 15, 16$ and 17 ($z \sim 12, 13$ and 14) for $\Delta\Omega \approx 0.1, 1$ and 10 deg^2 , respectively. All other considered cases exhibit intermediate behaviors. Note that, if we had considered other dust chemical compositions (e.g. UM-D-20, M-D-20, UM-ND-170, M-D-170, instead of UM-ND-20) which lead to lower M_{\min} (see Fig. 6), the redshift horizon would have moved towards even higher z .

We conclude that the redshift horizon at FIR wavelengths strongly depends on the properties of primordial dust and its host galaxy population. For $S = 1 \mu\text{m}$ and assuming a UM-ND-20 dust chemistry, metallicities $Z_g \gtrsim 5 \times 10^{-2} Z_{\odot}$ or dust fractions $D/M \gtrsim 0.06$

are required to reach the redshift horizon at $z > 7$ for $\Delta\Omega = 0.1 - 10 \text{ deg}^2$. However, these limits for Z_g and D/M could move towards lower values for different dust chemical compositions. For galaxies below such metallicity and dust fraction limits, gravitational lensing would be required to detect these fainter systems if sensitivity limits cannot be improved. We plan to explore the possibility of detecting gravitational lensing systems in a future study.

Fig. 10 summarizes our results regarding the redshift horizon as a function of sensitivity for a survey area of 1 deg^2 , considering the different galaxy parameters explored in Fig. 9. It is evident that an increase by one order of magnitude of Z_g , η or D/M , relaxes the sensitivity limit required for detection to similar order of magnitude. We have verified that similar trends are obtained if adopting survey areas of 0.1 and 10 deg^2 . Thus, observationally determining the redshift horizon for dust-emitting galaxies could constrain key properties of primeval galaxy populations.

Finally, we would like to point to encouraging discoveries in recent years of very rare massive sources in wide and shallow surveys, such as those expected to be carried out by near-future FIR telescopes. These objects seem to host massive reservoirs of dust in the early universe, while showing many similarities with local galaxies. Riechers et al. (2013), for example, reported the identification of a rare massive galaxy at $z \approx 6.3$, while searching 21 deg^2 of the *Herschel*/SPIRE data of the HerMES blank field survey at $250\text{-}500 \mu\text{m}$. For the brightest detected target, these authors estimated a FIR luminosity, an SFR ($\approx 2.9 \times 10^3 M_\odot \text{ yr}^{-1}$), and gas ($\approx 10^{11} M_\odot$) and dust ($\approx 1.3 \times 10^9 M_\odot$) masses 15-20 times those of the prototypical local ultra-luminous starburst Arp 220. They also reported a gas-to-dust ratio of ~ 80 and a highly enriched ISM for this object. More recently, Marrone et al. (2018) presented observations of a FIR luminous source at $z \approx 6.9$, which seems to be composed of two extremely massive star-forming galaxies. The larger of these systems shows an SFR of $\approx 2.9 \times 10^3 M_\odot \text{ yr}^{-1}$, a gas mass of $\approx 2.7 \times 10^{11} M_\odot$ and a dust mass of $\approx 2.5 \times 10^9 M_\odot$, being more massive than any other known galaxy at $z > 6$. In addition, its companion shows a stellar mass of $\approx 3.5 \times 10^{10} M_\odot$ and an SFR of $\approx 5.4 \times 10^2 M_\odot \text{ yr}^{-1}$, but with an order of magnitude less gas and dust. These authors suggested that these objects could be hosted by a dark-matter halo with a mass of more than $4 \times 10^{11} M_\odot$, which would be among the rarest systems at these early times. Also recently, Spilker et al. (2018) detected a massive molecular outflow from a gravitationally lensed DSFG, which likely resides in a dark matter halo of $\sim 10^{12} M_\odot$. The DSFG

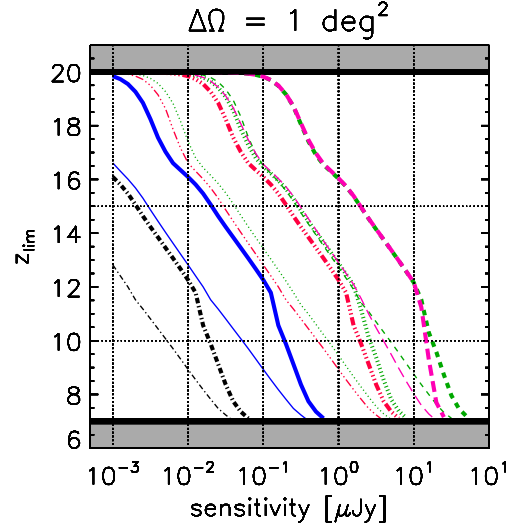


Figure 10. Impact of variations of different model parameters on the redshift horizon (compare with Fig. 8) for a survey area of 1 deg^2 . We only show results for the UM-ND-20 model, to emphasize the key features. Thin and thick lines are associated with the standard and shock size distributions, respectively. The reference model (solid blue line) corresponds to our standard parameters (De Rossi & Bromm 2017). The effects of variations of model parameters with respect to the standard model are shown with different line styles (see Fig. 9, for line style convention).

studied by Spilker et al. (2018) was discovered in the 2500 deg^2 South Pole Telescope Survey on the basis of its thermal dust emission and contains $\sim 1.2 \times 10^{10} M_\odot$ of molecular gas, $\sim 1.2 \times 10^8 M_\odot$ of dust and an SFR of $\sim 790 M_\odot \text{ yr}^{-1}$. According to earlier ALMA observations, this source is located at $z \approx 5.3$. Although challenging, the number of detected rare massive objects at very high z , with extremely high dust-to-gas ratios and high metallicities, will probably increase during future surveys with next-generation FIR telescopes, as our results indicate.

7. COMPARISON WITH ALMA AND NOEMA

For evaluating the potential improved capabilities of next generation FIR space telescopes to detect the first galaxies, we carry out an approximate comparison with current ground-based millimeter facilities, specifically ALMA and NOEMA. Furthermore, in Section 8, we analyse the potential synergy between such FIR telescopes and the *JWST*. In all cases, we consider the capability of each instrument to detect primeval sources for an ultra-deep exposure time of 10^6 s .

In the case of ALMA, we assume an optimum array configuration for highest sensitivity, obtained by using fifty 12m antennae. We consider observations within

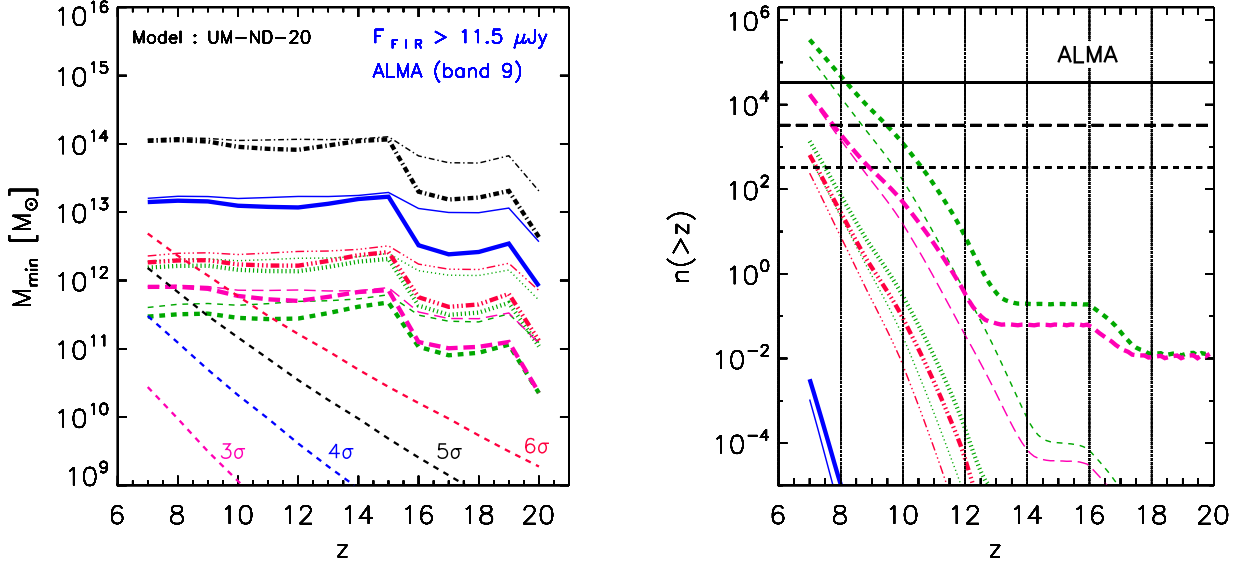


Figure 11. Similar to Fig. 9, but for ALMA band 9 (602- 720 GHz), assuming an array configuration of 50 (maximum value) 12-m antennae. A band-averaged sensitivity of $11.5 \mu\text{Jy}$ (10^6 s) has been assumed (sensitivity as a function of frequency was obtained from the ALMA on-line sensitivity calculator).

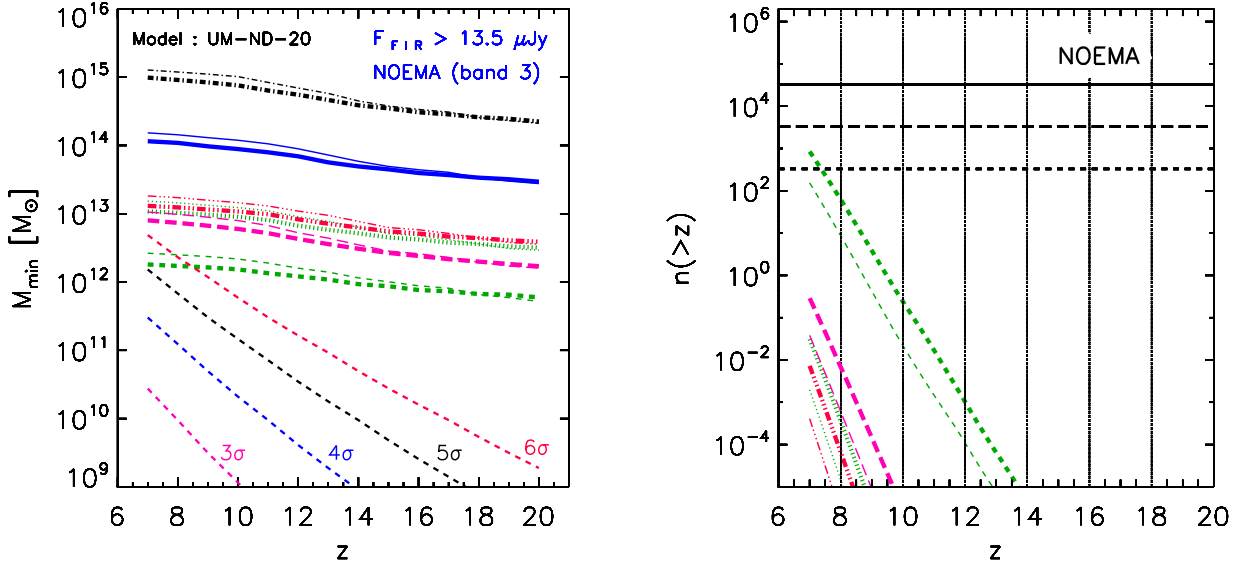


Figure 12. Similar to Fig. 9, but for NOEMA band 3 (200- 276 GHz). A band-averaged sensitivity of $13.5 \mu\text{Jy}$ (10^6 s) has been assumed.

the frequency range 602-720 GHz (ALMA, band 9). By using the ALMA on-line sensitivity calculator⁵ and considering a time integration of 10^6 s, we derive an average sensitivity of $11.5 \mu\text{Jy}$ for ALMA band 9. For 12 m antennae, an average field-of-view (FoV) of $\approx 0.02 \text{ arcmin}^2$ is obtained for the latter band. In the case of NOEMA,

we adopt the standard array configuration of eight 15 m antennae. We consider observations within the frequency range 200-276 GHz (NOEMA, band 3). For an exposure of 10 hr, NOEMA sensitivity is $\approx 70 \mu\text{Jy}$ for band 3. Thus, for an integration time of 10^6 s, we estimate a sensitivity of $\approx 13.5 \mu\text{Jy}$, assuming a scaling with the square root of the exposure time. Assuming these conditions, an average FoV of $\approx 0.09 \text{ arcmin}^2$ is obtained for NOEMA.

⁵ <http://almascience.eso.org/proposing/sensitivity-calculator>

By using the aforementioned parameters for ALMA and NOEMA, we performed a similar procedure to that described in Sec. 2 in order to obtain M_{\min} and n as a function of z . M_{\min} is defined as the lowest M_{vir} such that $F_{\text{FIR}} \geq 11.5 \mu\text{Jy}$ and $13.5 \mu\text{Jy}$, for ALMA and NOEMA, in their respective wavelength bands. Results for ALMA can be appreciated in Fig. 11, while Fig. 12 shows results for NOEMA. In the case of ALMA (NOEMA), $M_{\min} \gtrsim 10^{11} M_{\odot}$ ($M_{\min} \gtrsim 10^{12} M_{\odot}$) at $z \gtrsim 7$, even when assuming extremely high values of D/M , Z_g and η . These systems are very massive and rare, according to the statistics of the $\nu - \sigma$ peaks, rendering their detection challenging. We also note that $M_{\min}-z$ relations are smoother for NOEMA than for ALMA; this is due to the lower frequencies associated to NOEMA band 3, which is not affected by prominent spectral features (see Fig. 3).

In the right-hand panels of Fig. 11 and Fig. 12, we can see the number density of sources, $n(> z)$, as a function of z . The horizontal lines depict the regions corresponding to the redshift horizon, where $n(> z_{\text{lim}}) = 1/\Delta\Omega$, considering sky regions of $\Delta\Omega = 0.1$ (solid line), 1.0 (long-dashed line) and 10 deg^2 (dashed line), respectively. In the case of ALMA, models with $D/M \gtrsim 0.06$, $Z_g \gtrsim 5 \times 10^{-2} Z_{\odot}$ and $\eta = 0.1$ predict $n(> z) \gtrsim 1/10 \text{ deg}^2$ at $z \lesssim 10$, while, for NOEMA, only the model that assumes $\eta = 0.1$ reaches such values at $z \approx 7$. However, considering that the FoV of ALMA (NOEMA) is $\approx 0.02 \text{ arcmin}^2$ ($\approx 0.09 \text{ arcmin}^2$), it is clear that the probability of detecting sources within one FoV is negligible; even allowing for mosaicing, any detection will be very challenging.

Our results suggest that typical first galaxies hosting primordial dust grains are generally too faint for detection with current ground-based millimeter facilities. The development of next-generation telescopes is thus crucial to enhance the prospects of reaching these elusive sources.

8. COMPARISON WITH THE JWST

In order to evaluate the potential synergy between next-generation FIR telescopes and the *JWST*, we carry out a rough comparison between our predictions for a future telescope at FIR wavelengths with those derived for the *JWST* at NIR wavelengths. When comparing with the *JWST*, as our model does not include the physical prescriptions required to model the observed NIR radiation self-consistently, we obtain a rough estimate of upper limits for the NIR observed fluxes by simply analysing the stellar emission of our primordial systems.

Our dust model was developed with the aim of studying the FIR/sub-mm signatures associated with primor-

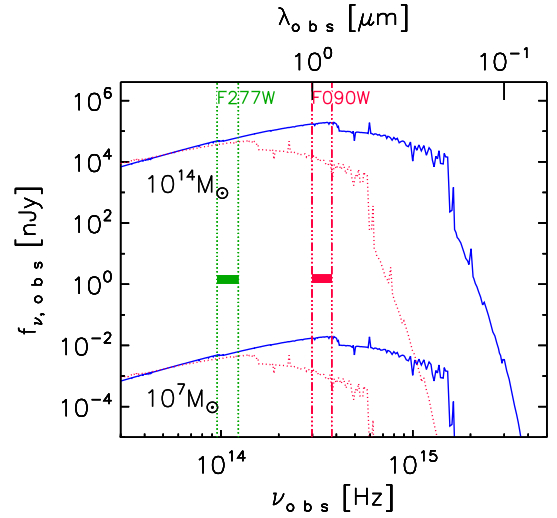


Figure 13. Observed fluxes from stellar clusters hosted by halos of $M_{\text{vir}} = 10^{14} M_{\odot}$ ($M_* \approx 1.8 \times 10^{11} M_{\odot}$, upper curves) and $M_{\text{vir}} = 10^7 M_{\odot}$ ($M_* \approx 1.8 \times 10^4 M_{\odot}$, lower curves) at $z = 20$ (red dotted curves) and $z = 7$ (blue solid curves). Vertical lines indicate the wavelength ranges associated with filters F277W and F090W of the NIRC2 instrument on *JWST*. The horizontal lines within each filter range depict the associated sensitivity for an exposure time of 10^6 s. This sensitivity together with a FoV of 10 arcmin^2 were used to estimate the critical mass M_{\min} and the number of detected sources N , as a function of z .

dial galaxies and, hence, it is focused on the physics of dust emission. As discussed in De Rossi & Bromm (2017), the model does not include the explicit physical prescriptions required to model observed spectra in NIR wavebands, such as nebular emission or the reprocessing of Lyman- α photons in the IGM. Thus, to obtain a rough estimate of the NIR luminosities of our sources, we evaluate the fluxes associated with the stellar component of our model galaxies, as a function of z and M_{vir} . For simplicity, we assume negligible extinction, so that the predicted fluxes represent upper limits.

According to some high- z observations (e.g., Fudamoto et al. 2017, and references therein), typical observed IR-to-UV ratios range between ~ 0.1 and ~ 100 at $M_* \sim 10^9 - 10^{12} M_{\odot}$.⁶ At similar masses and for our fiducial model parameters (see Sec. 2), we obtain IR-to-UV ratios⁷ ranging between ~ 0.001 and ~ 1 , depending

⁶ We emphasize that these values correspond to upper limits in many cases.

⁷ We define the IR-to-UV ratio as $L_{\text{IR}}/L_{\text{UV}}$, where L_{IR} corresponds to rest-frame bolometric dust luminosity at $\lambda = 8 - 1000 \mu\text{m}$, and L_{UV} is the rest-frame stellar luminosity at 1600 \AA with $L_{\text{UV}} = \nu(1600 \text{ \AA})L_{\nu}(1600 \text{ \AA})$.

on mass, z and dust model. As we are modelling the first galaxies hosting dust grains, our dust densities are very low. It is thus expected to obtain low IR-to-UV ratios, compared to galaxies in more advanced evolutionary stages, such as those currently observed. We note, however, that an increase in the dust-to-metal ratios, gas metallicities and/or star formation efficiencies of our model sources leads to an increase in the IR-to-UV ratios, reaching values similar to those currently observed at high z for the extreme cases considered in Sec. 6.

In Fig. 13, we show the observed specific fluxes associated with stellar clusters hosted by systems of $M_{\text{vir}} = 10^7 M_{\odot}$ ($M_* \approx 1.8 \times 10^4 M_{\odot}$, lower curves) and $M_{\text{vir}} = 10^{14} M_{\odot}$ ($M_* \approx 1.8 \times 10^{11} M_{\odot}$, upper curves) at $z = 7$ (blue solid curves) and $z = 20$ (red dotted curves). We evaluate the probability of detecting these systems with the Near Infrared Camera (NIRCam) F277W and F090W filters on board the *JWST*. The wavelength ranges and sensitivity levels (for an exposure time of 10^6 s) associated with the filters are indicated in Fig. 13 by using vertical and horizontal lines, respectively. For estimating M_{min} and N , we follow a similar approach to that described in Sec. 2. We calculate the average NIR flux (F_{NIR}) within each filter by using an expression similar to Equ. 5, and define M_{min} as the lower virial mass, such that F_{NIR} is above the sensitivity level within each filter. In order to estimate N , we assume a FoV of $\Delta\Omega = 10 \text{ arcmin}^2$ for the NIRCam instrument.

Predictions for the *JWST* are shown in Fig. 14. We can see that $M_{\text{min}} \gtrsim 10^9 M_{\odot}$ for both the F277W and F090W NIRCam filters, along the entire redshift interval considered. In particular, $M_{\text{min}} \sim 3 \times 10^9 M_{\odot}$ for filter F277W, not exhibiting significant variations with z , as expected from Fig. 13, since the specific flux within this filter barely evolves. On the other hand, M_{min} decreases from $10^{10} M_{\odot}$ at $z \approx 20$ to $10^9 M_{\odot}$ at $z \approx 7$ in the case of filter F090W, because of the increase of the specific flux within its associated wavelength range as z decreases. For our default model parameters, similar M_{min} could be achieved in the FIR for sensitivities $S \sim 1 \text{ nJy}$ (Fig 5), which are probably too low to be reached in the next decades. However, as previously discussed, galaxy populations with higher metallicities, dust fractions and/or star formation efficiencies could be detected at the FIR for higher sensitivity values.

As can be seen in the right-hand panel of Fig. 14, the redshift horizon for the *JWST* is reached at $z \approx 15$ for filters F090W and F277W. These findings suggest that upcoming observations in the NIR with the *JWST* could help to guide possible later surveys in the FIR with the next-generation telescopes. The synergy between such

facilities could be crucial to elucidate the first galaxies at these early times. However, it is worth highlighting again that the comparisons presented in this section should be taken with a grain of salt, as our model is not explicitly designed to model the observed NIR radiation.

9. SUMMARY AND CONCLUSIONS

In this study, we explore the prospects of detecting the dust continuum emission from first galaxy populations with next-generation FIR telescopes. Specifically, we apply the dust model developed by De Rossi & Bromm (2017) to estimate the least massive FIR/sub-mm sources that such facilities would be able to detect. We also predict the redshift horizons to detect at least one source within potential survey regions. As the design concepts for future FIR telescopes are evolving, we focus on a generic instrument, exploring a wide range of plausible sensitivities and survey areas. Our goal is to provide a baseline of exploration for future FIR campaigns, applicable to different sets of instrument parameters. Our main results can be summarized as follows:

- For systems of similar masses, higher dust temperatures are obtained at higher z (Fig. 2). This is caused by the increased intensity of the CMB radiation at earlier epochs. In addition, at higher z , systems of a given mass are more concentrated and exhibit higher central dust densities, which contribute to more efficient heating by the central stellar cluster.
- Because of the increase of dust temperature at higher z , galaxies of similar masses tend to be brighter at FIR/sub-mm wavelengths as z increases (Fig. 3 and 5). This effect leads to an extremely negative K-correction for these FIR/sub-mm sources, compensating and even reversing the decrease of the observed flux with the distance to the source (Fig. 4).
- As a consequence of the strong negative K-correction, the threshold virial mass that a generic FIR telescope would be able to detect during a survey campaign reaches a minimum at $z > 12$. For an instrument sensitivity $S = 1 \mu\text{Jy}$, $M_{\text{min}} \approx 1 - 2 \times 10^{12} M_{\odot}$ for the standard dust size distribution, and $M_{\text{min}} \approx 3 - 4 \times 10^{11} M_{\odot}$ for the shock size distribution (Fig. 6). Interestingly, we also found that at $7 < z < 12$ and for some dust models, the threshold mass increases towards lower z . This latter unexpected result is driven by different spectral features that enter the assumed

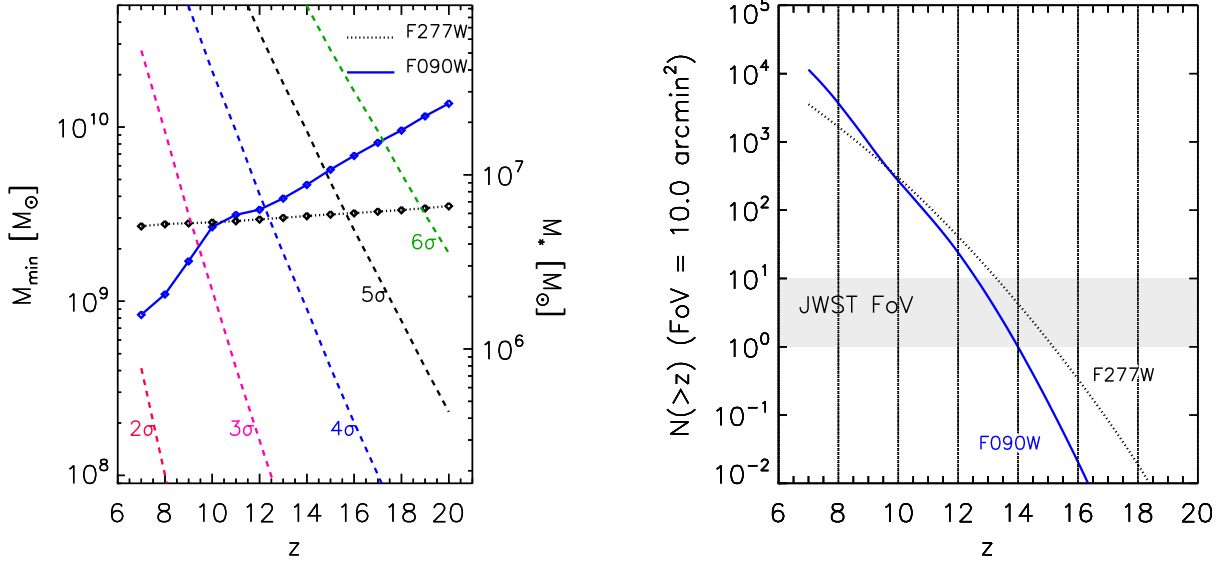


Figure 14. Deep surveys with the *JWST*. M_{\min} (left-hand panel) and N (right-hand panel) as a function of z , obtained when using the NIRCam F277W and F090W filters. In the left-hand panel, the right vertical axis shows M_* as a reference. In the right-hand panel, a $\text{FoV} = 10 \text{ arcmin}^2$ has been adopted. Although this is a rough estimate of the possible contribution of the stellar sources to the NIR radiation, we see that the number of detected sources per FoV reaches 1-10 at $z \sim 15 - 13$. Thus, observations in the NIR could help to guide possible surveys with next-generation FIR telescopes.

photometric filter as z increases. Different sensitivity values lead roughly to similar trends but with an increase of the absolute normalization of M_{\min} for higher S (Fig. 5).

- Although the strong negative K-correction associated with the first galaxies would contribute to their detection, these galaxies are located in very rare overdensities. Thus, they will be difficult to detect in blind surveys. Gravitational lensing might boost detectability, to be explored in future work.
- Variations from our fiducial values for dust-to-metal ratio (0.005 -default-, 0.06, 0.4) gas metallicity (5×10^{-4} , 5×10^{-3} -default-, $5 \times 10^{-2} Z_{\odot}$), or star formation efficiency (0.01 -default-, 0.1), can change the minimum halo mass needed for detection by more than two orders of magnitude (Fig. 9, left-hand panel).
- The probability of detecting one individual *typical* first galaxy during a potential FIR survey depends mainly on the instrument sensitivity (S) and, secondly, on the survey area ($\Delta\Omega$) (Fig. 7). In the case of the shock size distribution, the redshift horizon for $S \sim 1 \mu\text{Jy}$ is reached at $z \sim 7 - 10$, with the exact value depending on $\Delta\Omega$ and dust chemical composition. In the case of the standard size distribution, the redshift horizon for $S \sim 1 \mu\text{Jy}$

only reaches $z \sim 7$ for $\Delta\Omega = 10 \text{ deg}^2$ and for some particular dust chemistries. For instrument sensitivities $S \lesssim 0.1 \mu\text{Jy}$ and $\Delta\Omega \gtrsim 0.1 \text{ deg}^2$, all dust models predict a redshift horizon above $z \approx 7$.

- Interestingly, for all dust models, the redshift horizon decreases roughly linearly with $\log_{10}(S)$ at $z > 12$, exhibiting a similar slope of ≈ 4 (Fig. 8). At $z < 12$, some models predict departures from such linear relation as different spectral features enter the adopted FIR band.
- The FIR redshift horizon strongly depends on the properties of primordial dust and its host galaxy population. Considering that the nature of systems hosting primordial dust is very uncertain, with some recent studies suggesting high dust fractions in massive galaxies already at early epochs, we explore the effects of varying some critical galaxy properties such as gas metallicity, dust fractions and the star formation efficiency (Fig. 9 and 10). For $S = 1 \mu\text{Jy}$ and assuming a UM-ND-20 dust chemistry, metallicities $Z_g \gtrsim 5 \times 10^{-2} Z_{\odot}$ or dust fractions $D/M \gtrsim 0.06$ are required to reach the redshift horizon at $z > 7$ for $\Delta\Omega = 0.1 - 10 \text{ deg}^2$. However, these limits could move towards lower values for different dust chemical compositions. For galaxies below such metallicity and dust fraction limits, gravitational lensing

would be required to detect these fainter systems if sensitivity limits cannot be boosted.

- In general, an increase by one order of magnitude of Z_g , η or D/M , similarly relaxes the sensitivity limit required for the galaxy population to reach the redshift horizon at a given z (Fig. 10).
- Typical first galaxies hosting primordial dust grains seem to be too faint to be detected by current ground-based millimeter facilities, such as ALMA and NOEMA (see Fig. 11 and 12). Next-generation FIR telescopes are thus likely to play an important role in searching for these elusive sources.
- Although our model is not specifically designed to describe the NIR radiation from primeval galaxies, a rough estimate suggests a redshift horizon of $z \sim 15$ for the *JWST* NIRC*am* instrument (Fig. 14). Hence, observations with the *JWST* in the near future could guide follow-up surveys with next-generation FIR telescopes.

We conclude that the detectability of the dust continuum emission from first galaxies as FIR/sub-mm sources is boosted by an extremely negative K-correction. However, as these systems would reside in rare high-density peaks, their detection in blind surveys will be challenging. Such programs would require the development of techniques to address confusion noise. In particular, the detection of extremely faint sources could likely require flux amplification by gravitational lensing. Finally, taking into account the sensitivity of the FIR redshift horizon to the assumed dust properties, measurements of FIR/sub-mm source densities at $z > 7$ would shed light on the nature of dust at the very dawn of star formation.

We thank the anonymous referee for constructive comments, which helped to improve this paper. We also thank Alexander Ji for providing tabulated dust opacities for the different dust models used here. This work makes use of the Yggdrasil code (Zackrisson et al. 2011), which adopts Starburst99 SSP models, based on Padova-AGB tracks (Leitherer et al. 1999; Vázquez & Leitherer 2005) for Population II stars. VB acknowledges support from NSF grant AST-1413501. MEDR is grateful to PICT-2015-3125 of ANPCyT (Argentina) and also to María Sanz and Guadalupe Lucia for their help and support.

REFERENCES

- Asano, R. S., Takeuchi, T. T., Hirashita, H. & Inoue, A. K. 2011, ASP Conf., Ser. "Why Galaxies Care about AGB Stars II, ed. Kerschbaum, Lebzelter, & Wing, 445, 523
- Barkana, R., & Loeb, A. 2007, Reports on Progress in Physics, 70, 627
- Baugh, C. M., Lacey, C. G., Frenk, C. S., et al. 2005, MNRAS, 356, 1191
- Behroozi, P., Wechsler, R. H., Hearin, A. P., et al. 2019, MNRAS, 1134
- Bianchi, S., & Schneider, R. 2007, MNRAS, 378, 973
- Bromm, V. 2013, Asociacion Argentina de Astronomia La Plata Argentina Book Series, 4, 3
- Bromm, V., & Larson, R. B. 2004, ARA&A, 42, 79
- Bromm, V., & Yoshida, N. 2011, ARA&A, 49, 373
- Bromm, V., Yoshida, N., Hernquist, L., & McKee, C. F. 2009, Nature, 459, 49
- Burkert, A. 1995, ApJL, 447, L25
- Carilli, C. L., Murphy, E. J., Ferrara, A., & Dayal, P. 2017, ApJ, 848, 49
- Casey, C. M., Narayanan, D., & Cooray, A. 2014, PhR, 541, 45
- Cen, R., & Kimm, T. 2014, ApJ, 782, 32
- Cherchneff, I., & Dwek, E. 2010, ApJ, 713, 1
- Condon, J. J. 1974, ApJ, 188, 279
- Couchman, H. M. P., & Rees, M. J. 1986, MNRAS, 221, 53
- Davé, R., Finlator, K., Oppenheimer, B. D., et al. 2010, MNRAS, 404, 1355
- Dayal, P., & Ferrara, A. 2018, PhR, 780, 1
- De Rossi, M. E., & Bromm, V. 2017, MNRAS, 465, 3668
- De Rossi, M. E., Rieke, G. H., Shivaei, I., Bromm, V., & Lyu, J. 2018, ApJ, 869, 4
- Finlator, K., Davé, R., Papovich, C., & Hernquist, L. 2006, ApJ, 639, 672
- Fontanot, F., Monaco, P., Silva, L., & Grazian, A. 2007, MNRAS, 382, 903
- Fudamoto, Y., Oesch, P. A., Schinnerer, E., et al. 2017, MNRAS, 472, 483
- Furlanetto, S. R., Oh, S. P., & Briggs, F. H. 2006, PhR, 433, 181
- Gall, C., Hjorth, J., & Andersen, A. C. 2011, A&A Rv, 19, 43
- Greif, T. H., & Bromm, V. 2006, MNRAS, 373, 128
- Gruppioni, C., Ciesla, L., Hatziminaoglou, E., et al. 2017, PASA, 34, e055

- Jaacks, J., Finkelstein, S. L., & Bromm, V. 2018, *MNRAS*, 475, 3883
- Jeon, M., Pawlik, A. H., Bromm, V., & Milosavljević, M. 2014, *MNRAS*, 444, 3288
- Ji, A. P., Frebel, A., & Bromm, V. 2014, *ApJ*, 782, 95
- Kashlinsky, A., Mather, J. C., Helgason, K., et al. 2015, *ApJ*, 804, 99
- Laporte, N., Ellis, R. S., Boone, F., et al. 2017, *ApJL*, 837, L21
- Leitherer, C., Schaerer, D., Goldader, J. D., et al. 1999, *ApJS*, 123, 3
- Marrone, D. P., Spilker, J. S., Hayward, C. C., et al. 2018, *Nature*, 553, 51
- Mitchell-Wynne, K., Cooray, A., Gong, Y., et al. 2015, *Nature Communications*, 6, 7945
- Mortlock, D. J., Warren, S. J., Venemans, B. P., et al. 2011, *Nature*, 474, 616
- Muratov, A. L., Gnedin, O. Y., Gnedin, N. Y., & Zemp, M. 2013, *ApJ*, 772, 106
- Narayanan, D., Dey, A., Hayward, C. C., et al. 2010, *MNRAS*, 407, 1701
- Nozawa, T., Kozasa, T., Habe, A., et al. 2007, *ApJ*, 666, 955
- Oesch, P. A., Brammer, G., van Dokkum, P. G., et al. 2016, *ApJ*, 819, 129
- Oh, S. P., & Haiman, Z. 2002, *ApJ*, 569, 558
- Planck Collaboration, Ade, P. A. R., Aghanim, N., et al. 2014, *A&A*, 571, A16
- Pollack, J. B., Hollenbach, D., Beckwith, S., et al. 1994, *ApJ*, 421, 615
- Riechers, D. A., Bradford, C. M., Clements, D. L., et al. 2013, *Nature*, 496, 329
- Safronek-Shrader, C., Milosavljević, M., & Bromm, V. 2014, *MNRAS*, 438, 1669
- Schneider, R., Hunt, L., & Valiante, R. 2016, *MNRAS*, 457, 1842
- Sheth, R. K., Mo, H. J., & Tormen, G. 2001, *MNRAS*, 323, 1
- Silvia, D. W., Smith, B. D., & Shull, J. M. 2010, *ApJ*, 715, 1575
- Somerville, R. S., Gilmore, R. C., Primack, J. R., & Domínguez, A. 2012, *MNRAS*, 423, 1992
- Spilker, J. S., Aravena, M., Béthermin, M., et al. 2018, *Science*, 361, 1016
- Tegmark, M., Silk, J., Rees, M. J., et al. 1997, *ApJ*, 474, 1
- Todini, P., & Ferrara, A. 2001, *MNRAS*, 325, 726
- The OST mission concept study team. 2018, arXiv 1809.09702
- Valiante, R., Schneider, R., Bianchi, S., & Andersen, A. C. 2009, *MNRAS*, 397, 1661
- Vázquez, G. A., & Leitherer, C. 2005, *ApJ*, 621, 695
- Venemans, B. P., Findlay, J. R., Sutherland, W. J., et al. 2013, *ApJ*, 779, 24
- Venemans, B. P., Walter, F., Decarli, R., et al. 2017, *ApJ*, 837, 146
- Watson, D., Christensen, L., Knudsen, K. K., et al. 2015, *Nature*, 519, 327
- Wilkins, S. M., Feng, Y., Di Matteo, T., et al. 2018, *MNRAS*, 473, 5363
- Zackrisson, E., Rydberg, C.-E., Schaerer, D., Östlin, G., & Tuli, M. 2011, *ApJ*, 740, 13